NASA TECHNICAL NOTE

NASA TN D-7401

NASA TN D-7401

A FISSION GAS RELEASE CORRELATION FOR URANIUM NITRIDE FUEL PINS

by Michael B. Weinstein and Harry W. Davison

Lewis Research Center
Cleveland, Ohio 44135

NATIONAL AERONAUTICS AND SPACE ADMINISTRATION • WASHINGTON, D. C. • OCTOBER 1973

1. Report No.	2. Government Accession No.	3. Recipient's Catalog No.
NASA TN D-7401		

4. Title and Subtitle	5. Report Date
A FISSION GAS RELEASE CORRELATION FOR URANIUM NITRIDE FUEL PINS	October 1973
	6. Performing Organization Code

7. Author(s)	8. Performing Organization Report No.
Michael B. Weinstein and Harry W. Davison	E-7498
	10. Work Unit No. 503-05

9. Performing Organization Name and Address	11. Contract or Grant No.
Lewis Research Center National Aeronautics and Space Administration Cleveland, Ohio 44135	

12. Sponsoring Agency Name and Address	13. Type of Report and Period Covered
National Aeronautics and Space Administration Washington, D. C. 20546	Technical Note
	14. Sponsoring Agency Code

15. Supplementary Notes

16. Abstract

A model has been developed to predict fission gas releases from UN fuel pins clad with various materials. The model has been correlated with total release data obtained by different experimentors, over a range of fuel temperatures primarily between 1250 and 1660 K, and fuel burnups up to 4.6 percent. In the model, fission gas is transported by diffusion mechanisms to the grain boundaries where the volume grows and eventually interconnects with the outside surface of the fuel. The within grain diffusion coefficients are found from fission gas release rate data obtained using a sweep gas facility.

17. Key Words (Suggested by Author(s))	18. Distribution Statement
Fission gas Uranium mononitride	Unclassified - unlimited

19. Security Classif. (of this report)	20. Security Classif. (of this page)	21. No. of Pages	22. Price*
Unclassified	Unclassified	56	Domestic, $3.50 Foreign, $6.00

* For sale by the National Technical Information Service, Springfield, Virginia 22151

A FISSION GAS RELEASE CORRELATION FOR URANIUM NITRIDE FUEL PINS

by Michael B. Weinstein and Harry W. Davison

Lewis Research Center

SUMMARY

A mathematical model has been developed to predict fission gas release rates from uranium nitride (UN) fuel pins clad with various materials. Predicted and measured gas releases have been correlated for UN pins tested to 4.6-atom-percent fissions (burnup) at temperatures which primarily ranged from 1250 to 1660 K. Most of the fuel pins were clad with Nb-1Zr or PWC-11; however, several were clad with W-25Re or T-111.

The model assumes gas release from individual grains to the grain boundaries. For grains at the fuel surface, gas release is instantaneous. For grains inside the fuel, the gas collects at the grain boundaries where the gas volume grows and eventually interconnects with the outside surface of the fuel. The fraction of grain boundary porosity which has interconnected has been assumed to be proportional to the porosity, with the proportionality constant calculated from the gas release data. As a similifying assumption it is assumed that the pressure of the intergranular gas is equal to the fuel-clad contact pressure. Fuel and clad strength properties were used to calculate the contact pressure. Empirically, interconnection only occurs if the fuel is above a set of minimum temperature or burnup conditions. Diffusion coefficients for the intergranular transport of fission gas were calculated from fission gas release rate data measured in a sweep gas facility.

INTRODUCTION

Reliable methods to predict the amount of fission gas release are required for the most efficient design of space power reactor fuel elements. A program to develop these methods for uranium nitride (UN) fuel pins has been in progress at NASA Lewis Research Center.

Model development is difficult due to the complex and interacting fission gas transport and release processes operating in fissioning fuel elements. Carroll, in a recent

review (ref. 1), cites a multiplicity of different transport, trapping, and release mechanisms and models which have been used to explain fission gas behavior in fuels. Possible fission gas transport mechanisms include atomic diffusion, fission-enhanced diffusion, and gas bubble diffusion, all of which can be complicated by trapping and release processes.

Atoms diffusing through the fuel can be trapped by defects or by stationary gas bubbles. They can be released from these traps by defect annealing or by kinetic resolution from the bubbles. Similarly, bubbles diffusing under the influence of a driving force, such as a temperature gradient, may be trapped or delayed by solid fission product precipitates, dislocations, or grain boundaries. Release from these traps occurs when the driving force exceeds the retarding force.

These transport-trapping processes are themselves the product of multiple causes. As an example, Carroll (ref. 1) points out that possible bubble motion mechanisms are surface diffusion, volume (or bulk) diffusion, and evaporation-condensation. Domination of one bubble diffusion mechanism over the others depends on the material properties, the fuel temperature, and the bubble size (Nichols, ref. 2).

Fission gas release mechanisms include direct recoil (the ejection of fission-produced atoms from the fuel), knockout (ref. 3) (the ejection of gas and fuel atoms from the fuel surface by recoiling fission fragments), as well as the release when diffusing gas atoms or bubbles reach a free surface. Free surfaces include internal cracks or grain boundaries open to the exterior surface of the fuel.

Tests to study the variation of radioactive fission gas release rates from UN with three major test variables - temperature, fission-rate density, and burnup - were conducted using a sweep gas facility located at the NASA Plum Brook Reactor Facility. A description of the sweep gas facility has been given in reference 4.

In these experiments, small-size, high-enrichment UN samples were irradiated at high fission-rate densities at temperatures from 425 to 1780 K. Based on a preliminary diffusion transport model (atomic plus fission-enhanced diffusion with desorption and recoil release), equations were developed to relate measured fission gas release rates to the test variables. Unknown constants in these equations were evaluated from the data (ref. 5).

With the completion of additional tests and analyses, transport by bubble diffusion was added to the preliminary model, and the agreement between measured and calculated release rates improved.

In actual fuel pins, the restraining effect of the fuel element clad has a significant effect on fuel swelling (ref. 6) and would also be expected to significantly affect fission gas release. CYGRO-3 (ref. 7) a new fuel rod performance program includes this clad restraint effect on gas release by linking gas release to bubble size which is in turn dependent on fuel element stresses.

Fission gas release from fuels has been linked to the interconnection of grain boundary porosity. Carroll (ref. 1) mentions the interconnection concept as is used to explain UN behavior, while Ainscough (ref. 8) pictorially shows the development of intergranular bubbles and cracks in UO_2.

We have developed a model relating gas release to the amount of interconnected grain boundary porosity, the growth of which depends on the fuel stress as determined by the fuel-clad contact pressure.

RESULTS AND DISCUSSION

Equations have been developed and correlated with measured fission gas releases from UN fuel pins representing various fuel-clad combinations. The development of these equations can be summarized as follows:

First the release rates of radioactive fission-product noble gas isotopes (krypton and xenon) from four UN fuel specimens were measured using a helium sweep gas facility, a description of which is given in reference 4. (Test operations, data-taking procedures, preliminary analyses and observations are discussed in ref. 5. Pertinent sweep gas data is presented in appendix A.) The measured krypton-88 (Kr^{88})[1] release rates were then correlated with a gas release equation which was derived by considering diffusional transport and release from fuel specimens. Three separate diffusion mechanisms are included in the gas release model: fission-enhanced diffusion, atomic diffusion, and bubble "diffusion" (bubble motion caused by surface diffusion).

The postirradiation photomicrographs of our irradiated fuel specimens show extensive interconnection of intergranular porosity for the specimens operated at ~1500 K or higher. Hence, we linked gas release from these specimens to the gas release from individual grains to the grain boundaries.

The model which was then developed to represent the release of stable (nonradioactive) gas from clad fuel pins considers gas (at a constant pressure) being released to the individual grain boundaries where the gas volume increases and eventually interconnects to the outside. As simplifications we assume all the fuel porosity to be located at the grain boundaries, and assume the amount of interconnected porosity to be proportional to the porosity. We also assume that the pressure of the intergranular gas is equal to the fuel-clad contact pressure which can be approximately calculated from fuel and clad creep strength and other material properties. The stable gas release model is then correlated with data obtained from various sources.

[1]Krypton-88 is used for most of our experimental analysis because its 2.4-MeV gamma ray is easiest to monitor and count.

The detailed derivations of all the correlation equations are carried out in appendixes B, C, and D. The stable gas release data from outside sources is listed in appendix E.

Radioactive Fission Gas Release Rate Correlation

In an earlier report (ref. 5) Kr^{88} release rates from three UN specimens were correlated with the predictions of a preliminary fission gas transport-release model which included the mechanisms of atomic diffusion, fission-enhanced diffusion, and direct recoil release. Postirradiation photomicrographs of the fuel specimens indicated that bubble migration was also a probable gas migration mechanism, and that gas transport was first to the grain boundaries (fig. 1), then out of the pin. Additional gas release data from a fourth UN specimen (capsule 124) reinforced the earlier conclusions. Data

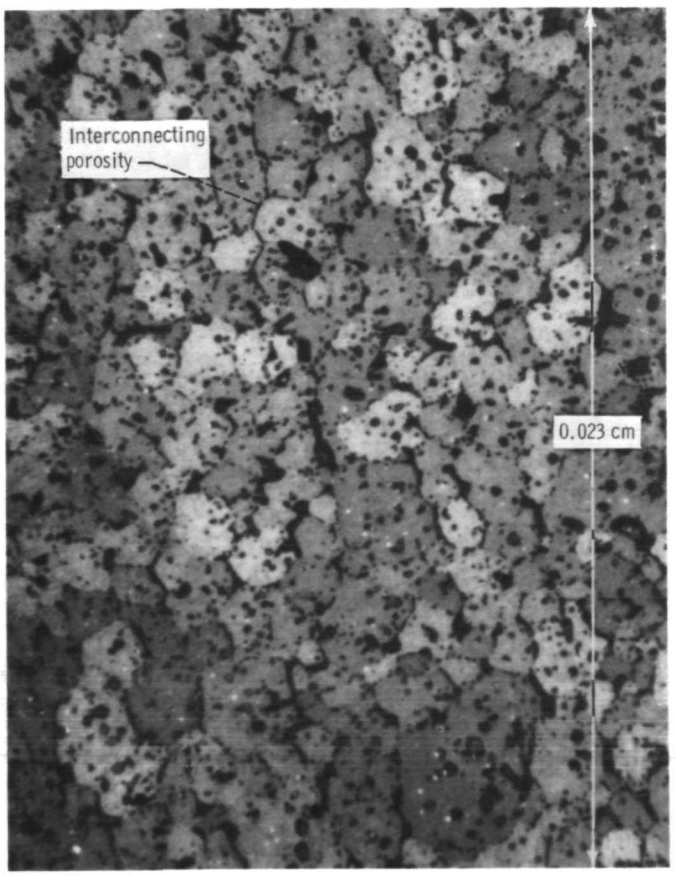

Figure 1. - Section of fuel pin in capsule 123. X500.

TABLE I. - OUTLINE OF IRRADIATION TESTS

Capsule	Total irradiation time, hr	Total burnup, percent	Primary test temperature, K	Temperature range (side thermocouple), K	Fission-rate density range, $\frac{\text{fissions}}{\text{cm}^3\text{-sec}}$	Number of sweep gas samples
121	1294	8.3	1780	1215 to 1789	$3.34 \text{ to } 8.29\times10^{14}$	9
122	1923	6.6	1223	593 to 1225	.71 to 3.64	19
123	1894	6.0	1505	579 to 1512	.49 to 4.45	19
124	1751	7.8	Several	[a]425 to 1323	.36 to 7.57	15
				[b]525 to 1357	.35 to 3.15	11

[a]Helium sweep gas.
[b]Neon sweep gas.

for all four capsule tests is presented in table I and in detail in appendix A.

The derivation of the following fission gas release rate equation which includes a term for bubble motion is presented in appendix B:

$$R_{pin} = (1 + \alpha_4 b)\left[\frac{\alpha_3 YSLf}{4T} + fYS\left(\frac{D_{fo}f + D_o e^{-Q_o/RT} + \frac{\alpha_2 f}{K_1^2 T^2} e^{-Q_s/RT}}{\lambda}\right)^{1/2}\right] \quad (1)$$

where $b > 1.5$ percent. (Symbols are defined in appendix F.)

The bubble motion term in equation (1) which is

$$\frac{\alpha_2 f}{K_1^2 T^2} e^{-Q_s/RT}$$

is an approximation which neglects bubble growth, size dependent velocity, and gas transport to and from the matrix. The term does include power, thermal conductivity, and temperature dependences.

Equation (1) contains seven unknown constants: α_4, α_3, $D_{fo}S^2$, $D_o S^2$, Q_o, $\alpha_2 S^2$, and Q_s. The values for these constants were obtained by conducting a least-squares

fitting analysis on equation (1) and the Kr^{88}-helium release rate data given in appendix A. Steps outlining the use of such a least-squares analysis with a nonlinear equation, such as equation (1), are presented in appendix C.

The resulting gas release equation is

$$R_{pin} = (1 + 0.376b)\left[\frac{3.65\times10^{-3}Yf}{T} + \frac{fY}{\lambda^{1/2}}\left(1.55\times10^{-29}f + 4.49\times10^{-9}e^{-\frac{18\,800}{T}} + \frac{1.89\times10^{-17}f}{K_1^2T^2}e^{-\frac{18\,400}{T}}\right)^{1/2}\right] \quad (2)$$

where $b > 1.5$ percent, $\alpha_2 = 0$ for capsules 122 and 124. Equation (2) is given next in terms of the activity of Kr^{88} in the sweep gas.

$$A_k = (1 + 0.376b)\left[\frac{3.07\times10^{-8}f}{4T} + f\left(1.59\times10^{-35}f + 4.61\times10^{-15}e^{-\frac{18\,800}{T}} + \frac{1.94\times10^{-23}f}{K_1^2T^2}e^{-\frac{18\,400}{T}}\right)^{1/2}\right] \quad (3)$$

where $A_k = R_{pin}(Kr^{88})/4.285\times10^3$, $\lambda = 6.877\times10^{-5}$ second^{-1}, and $Y = 3.6\times10^{-2}$. The constant 4.285×10^3 arises from the decay of Kr^{88} in traveling from the fuel specimen to the detector. The calculated activities are compared graphically to our data in figure 2. For convenience, calculated values for all of the data points are included in the appropriate tables of appendix A.

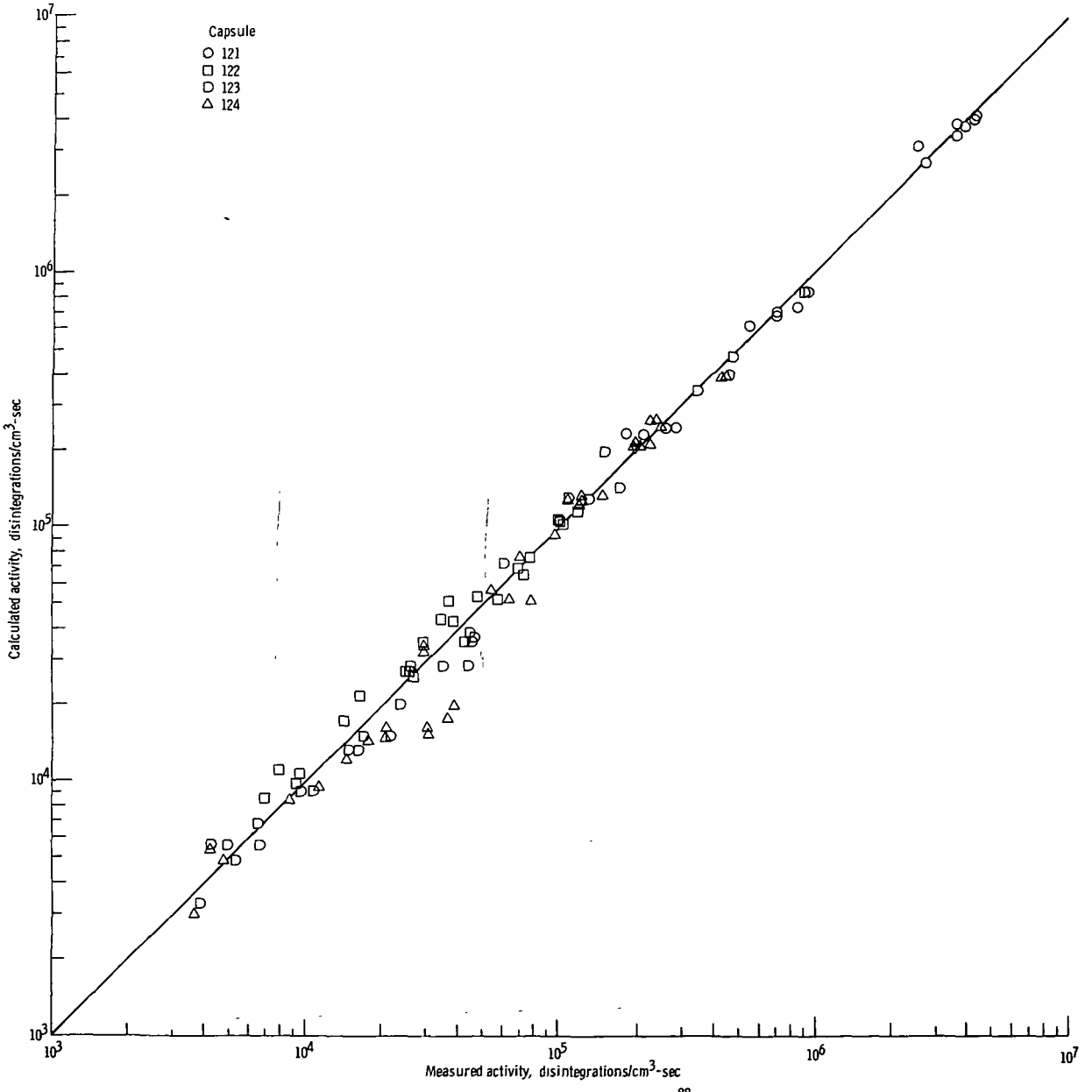

Figure 2. - Comparison of measured and calculated Kr^{88} activities.

For the data points included in figure 2, the mean absolute relative difference,

$$\frac{1}{n}\sum\left|\frac{A_{k,\text{measured}} - A_{k,\text{calculated}}}{A_{k,\text{measured}}}\right|$$

is 13.8 percent, and the standard deviation is 11.1 percent.

As noted in equation (2), we found that a good correlation between the derived equation (1) and the data required that $\alpha_2 = 0$ for the data from capsules 122 and 124. This indicates, as will be discussed later on, that bubble motion was not an important transport mechanism for these two capsules.

Some of the capsule 124 tests were conducted using neon (Ne), instead of helium (He), as the sweep gas. In this manner we were able to test this particular fuel specimen at different power-temperature combinations.

As reported in previous reports (refs. 4 and 5), the capsule used for our sweep gas tests contains a heat transfer gas gap between the fuel specimen and the capsule wall. Thus a capsule containing a particular gas gap width would have a set fuel power-temperature relation. Changing the sweep gas from helium to neon drastically changed the gap conductivity and allowed us to run tests on capsule 124 at:

(1) The same temperature, but widely different power densities, or

(2) The same power density, but different temperatures.

Release rate data for capsule 124 is presented in tables V(d) and VI of appendix A. This data was not used to obtain the constants for equation (2) but does serve as a good check on the temperature and fission rate density dependences.

A modified form of equation (2) was used to calculate Kr^{88} release rates into the neon sweep gas. Modification was necessary because the recoil constant, 3.65×10^{-3} in equation (2), found for helium, had to be altered to account for the increased relative stopping power of neon. Using values from Evans (ref. 9) the increase in the value of the recoil constant is a factor of 3.29 when changing from 99.8 percent He-0.2 percent A to 90 percent No-0.2 percent A (neon gas composition).

For the Kr^{88} release into neon calculations, the modified form of equation (3) becomes

$$A_k = (1 + 0.376b)\left[2.52\times10^{-8}\,\frac{f}{T} + f\left(1.59\times10^{-35}f + 4.61\times10^{-15}e^{-\frac{18\,800}{T}}\right)^{1/2}\right] \qquad (4)$$

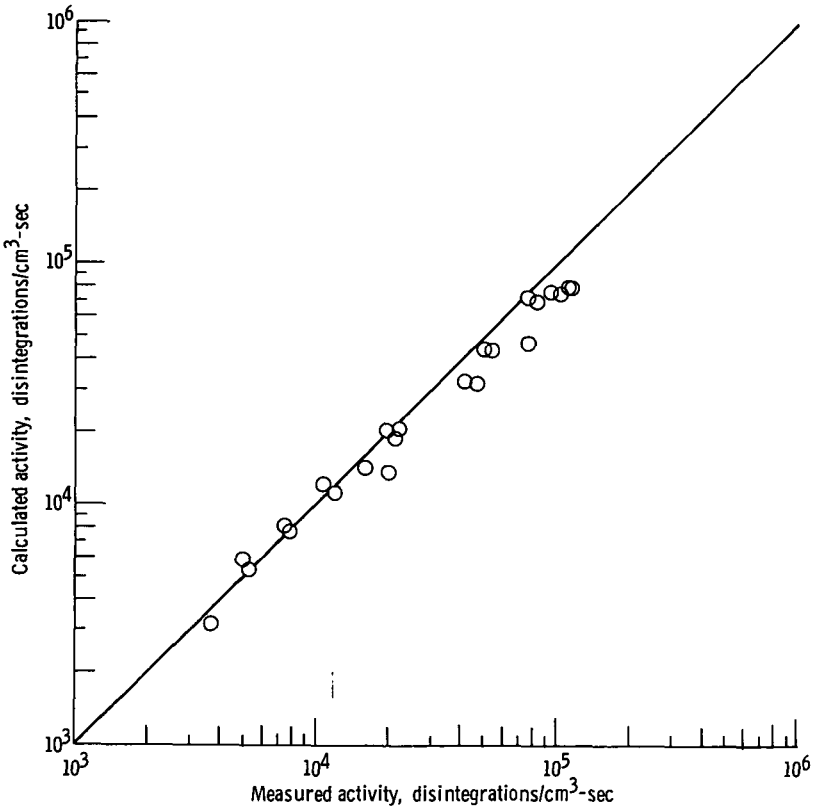

Figure 3. - Comparison of measured and calculated Kr^{88} activities in neon sweep gas.

where there is no bubble motion term.

Calculated and measured Kr^{88} release rates into neon are shown in figure 3. The mean relative difference is 10.6 percent, and the standard deviation of the relative difference is 13.7 percent.

The derivation of an equation to predict stable fission product gas releases from rectangular grains was carried out in reference 5. The result in terms of total release divided by total birth is

$$\left(\frac{R_T}{B}\right)_g = 1 - \frac{8}{\pi^2} \sum_{n=0}^{\infty} \frac{1 - e^{-(2n+1)^2 \frac{D\pi^2 t}{4y_2^2}}}{(2n+1)^4 \frac{D\pi^2 t}{4y_2^2}} \qquad (5)$$

$$D = D_{fo}f + D_o e^{-Q_o/RT} + \alpha_2 e^{-Q_s/RT} \frac{f}{T^2 K_1^2}$$

(from eqs. (B5) and (B7)) and recoil release has been neglected.

For equation (5) to be useful, values must be obtained for the diffusion constants D_{fo}, D_o, and α_2. Values obtained for the diffusion terms in equation (1) contain the nonseparable surface area factor S^2.

If we assume, as was done in reference 5, that after approximately 6 percent burnup we have attained complete interconnection of circumferential intergranular porosity as in capsules 121 and 123 (fig. 1), S^2 is approximately 200 centimeters^4, and D becomes the following:

$$D = 8.22\times10^{-31}f + 2.37\times10^{-10} e^{-\frac{18\,800}{T}} + 1.00\times10^{-18} \frac{f}{K_1^2 T^2} e^{-\frac{18\,400}{T}} \tag{6}$$

For calculational purposes, equation (5) can be approximated by

$$\left(\frac{R_T}{B}\right)_g = \begin{cases} 0.479\eta^{1/2} & \text{for } \eta < 1 \\ 1 - \frac{8}{\pi^2}\left(\frac{1}{\eta} + \frac{1}{81\eta} + \frac{1}{625\eta} + \frac{1}{2401\eta} - \frac{e^{-\eta}}{\eta}\right) & \text{for } \eta > 1 \end{cases} \tag{7}$$

where $\eta = D\pi^2 t/4y_2^2$.

Stable Fission Gas Release Correlation

Equations relating stable fission gas release from UN fuel pins to the release from single grains have been derived (appendix D) and have been correlated with available UN test data.

The model used assumes fission gas release from individual grains to the grain boundaries. If a grain is at the fuel surface, that fission gas is immediately released from the pin. Gas is only released from the fuel interior through interconnected porosity

which forms as the amount of intergranular gas increases.

Two basic assumptions are that the intergranular gas is at a constant pressure, and that the fraction of porosity interconnected to the surface is proportional to porosity.

The following equation (derived as eq. (D8)) relates total gas release from the pin R_T/B to total gas release from a grain $(R_T/B)_g$:

$$\frac{R_T}{B} = \left(\frac{R_T}{B}\right)_g - \left[\frac{2P\left(1 - \frac{V_{g_0}\beta}{V_f}\right)}{3KT\beta fYt}\right]\left\{1 - \exp\left[\frac{-KT\beta fYt\left(1 - \frac{2y_2}{r_2 - r_1}\right)\left(\frac{R_T}{B}\right)_g}{P}\right]\right\} \quad (8)$$

where P is the constant gas pressure and β is the factor which defines the rate at which porosity interconnects, is interconnected porosity/total porosity, and is found from the data analysis. $(R_T/B)_g$ is found from equation (7).

The constant gas pressure P in equation (8) is assumed to equal the steady-state fuel-clad contact pressure which can be calculated from the following equation (derived as eq. (D(18) in appendix D):

$$P^{(n_c - n_f)} = \frac{A_F k_{4f}}{A_c k_{4c}} - \frac{1}{3}\frac{\dot{v}}{k_{4c} A_c P^{n_f}} \quad (9)$$

The basic assumptions used in deriving equation (9) were that both the fuel and clad are creeping at the same constant rate, tangential and axial stresses in the fuel and clad are proportional to radial stress, and the fuel volumetric strain rate can be approximated by the unrestrained fuel swelling strain rate (calculated from Lietzke, ref. 10).

The UN fuel pin data presented in appendix E were correlated with equation (8). The results of the correlation are shown in figure 4 for those pins which had a measured gas release of over 1 percent.

Calculated results for all the experiments are presented in table II. The average relative difference for all the data is 44.3, the standard deviation of the relative differences is 37 percent.

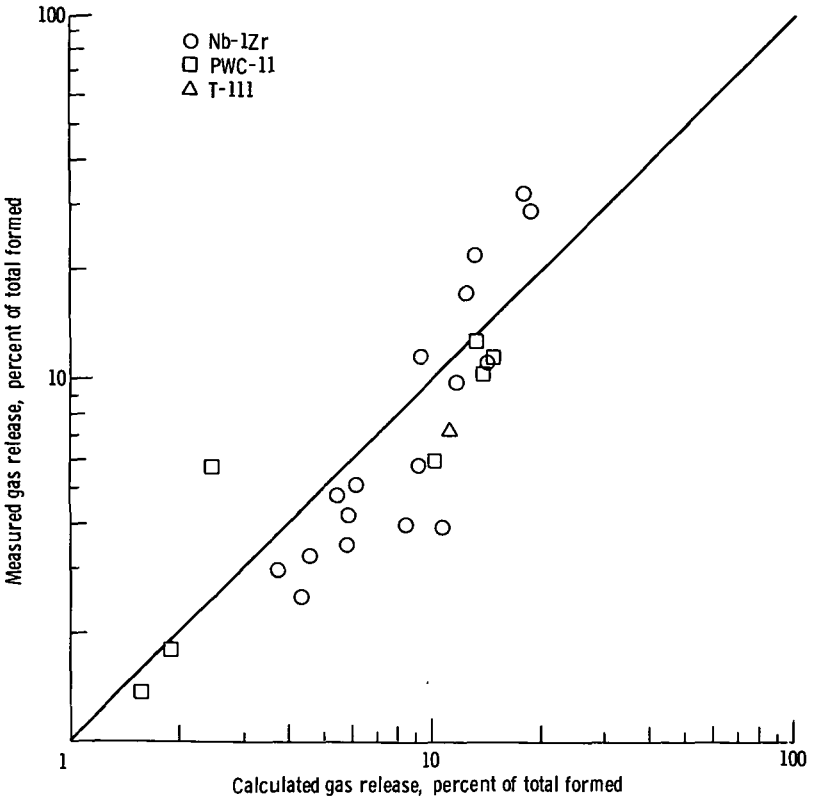

Figure 4. - Comparison of measured and calculated stable gas release from UN (high gas release data only).

For the data presented in figure 4, the average relative difference

$$\frac{1}{n}\sum \frac{\left(\frac{R_T}{B}\right)_{measured} - \left(\frac{R_T}{B}\right)_{calculated}}{\left(\frac{R_T}{B}\right)_{measured}} = -0.26$$

with a standard deviation of 0.52. For this data the best value of β, found by a least-squares analysis, is 9.73. This indicates that the porosity is completely interconnected when the total intergranular porosity reaches ~10 percent.

Empirically it was also apparent that good agreement between equation (8) and the data required that bubble motion occurs only at the higher temperatures and burnup rates and that pore interconnection occurred only above some minimum temperature and burnup. At low temperature and burnup the gas release comes only from that layer of grains touching the fuel surface.

TABLE II. - CALCULATED AND MEASURED STABLE GAS RELEASE DATA

Experiment	Fuel temperature, K	Burnup, percent	Burnup rate, percent / 10 000 hr	Model[a]	Contact pressure, N/cm^2	R_T/B, percent	
						Measured	Calculated[b]
1	1144	0.06	1.54	S	944	0.08	0.031
2	1248	.06	1.54	S	560	.09	.048
3	1443	.057	3.58	B	418	3.5	5.4
4	1422	.72	4.53	B	511	5.1	5.8
5	1477	.42	3.85	B	390	3.0	3.6
6	1533	.42	3.85	B	327	3.3	4.4
7	1533	.40	3.67	B	324	2.5	4.2
8	1429	1.20	7.10	B	601	4.8	5.2
9	1582	1.20	7.10	B	362	11.7	8.8
10	1443	1.21	7.16	B	593	4.2	5.5
11	1568	.58	6.82	B	398	.53	6.1
12	1658	.63	7.41	B	314	.88	7.5
13	1547	.61	7.17	B	441	.68	5.3
14	1533	2.26	8.22	B	541	9.9	11.1
15	1665	2.23	8.11	B	356	29.1	18.2
16	1581	2.34	8.51	B	481	11.1	13.6
17	1554	1.65	5.50	B	317	17.2	12.0
18	1637	1.82	6.01	B	268	32.3	17.3
19	1568	1.51	5.03	B	283	21.9	12.6
20	1616	.78	7.09	B	285	5.8	8.8
21	1665	.74	6.73	B	240	3.9	10.3
22	1588	.72	6.54	B	297	4.0	8.0
23	1348	.19	2.87	S	462	.1	.037
24	1470	.18	2.72	S	304	.1	.095
25	1483	.18	2.72	S	295	.1	.11
26	1403	.39	2.84	S	392	.1	.090
27	1470	.39	2.84	S	314	.2	.13
28	1458	.40	2.91	S	330	.2	.14
29	1265	.78	2.35	S	690	.05	.081
30	1408	.76	2.30	S	391	.1	.17

[a]Interconnection, I; bubble motion + interconnection, B; surface release, S.

[b]Interconnection factor $\beta = 8.75$.

TABLE II. - Concluded. CALCULATED AND MEASURED STABLE GAS RELEASE DATA

Experiment	Fuel temperature, K	Burnup, percent	Burnup rate, percent / 10 000 hr	Model[a]	Contact pressure, N/cm^2	R_T/B, percent	
						Measured	Calculated[b]
31	1388	0.78	2.36	S	438	0.06	0.17
32	1240	2.54	4.88	S	3760	.05	.11
33	1350	2.54	4.88	S	2500	.37	.17
34	1285	2.54	4.88	S	3120	.09	.13
35	1475	1.18	1.18	S	975	.34	.39
36	1460	1.43	1.36	S	1070	.04	.38
37	1543	.70	2.20	S	991	.09	.29
38	1538	.60	1.89	S	963	.03	.29
39	1538	.60	1.89	S	963	.11	.29
40	1538	.60	1.89	S	963	.13	.29
41	1480	1.08	1.10	S	947	.14	.40
42	1460	1.08	1.10	S	996	.09	.37
43	1558	.07	.65	S	698	.05	.28
44	1363	1.16	1.13	S	1330	.01	.24
45	1498	1.16	1.13	S	924	.08	.44
46	1488	1.16	1.13	S	947	.04	.42
47	1228	4.58	4.78	I	4160	1.36	1.50
48	1332	4.58	4.78	I	2730	5.96	2.37
49	1275	4.58	4.78	I	3450	1.78	1.83
50	1473	.78	1.26	S	979	.02	.31
51	1478	.78	1.26	S	966	.03	.31
52	1160	2.72	2.63	S	4000	.05	.097
53	1300	2.72	2.63	S	2170	.13	.18
54	1255	2.72	2.63	S	2620	.12	.15
55	1497	1.12	1.10	S	908	.06	.44
56	1443	4.17	3.48	B	1640	6.0	9.9
57	1503	4.17	3.48	B	1392	10.3	12.8
58	1528	4.17	3.48	B	1304	11.5	14.2
59	1503	4.17	3.48	B	1392	12.6	12.8
60	1393	1.78	2.16	S	4635	.14	.30
61	1598	1.45	2.50	S	676	.10	.59
62	1920	1.75	3.01	B	506	7.10	10.8
63	1255	.47	.58	S	1570	.05	.14
64	1270	.89	1.10	S	5200	.10	.15
65	1271	.92	1.14	S	5220	.10	.15

[a]Interconnection, I; bubble motion + interconnection, B; surface release, S.
[b]Interconnection factor $\beta = 8.75$.

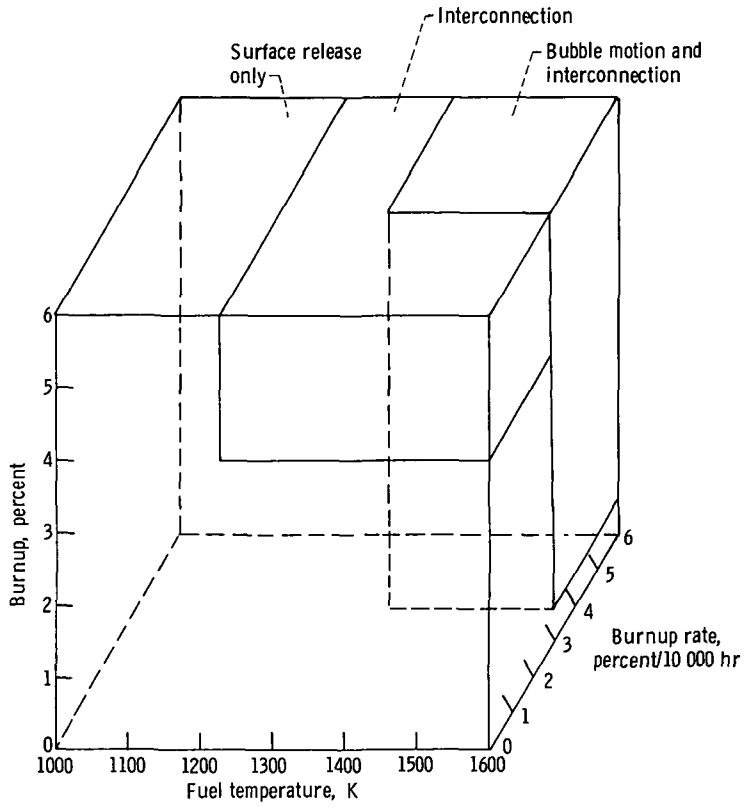

Figure 5. - Regions of interconnection and bubble motion.

The data indicate that: Bubble motion exists if the fuel temperature exceeds 1375 K, the burnup exceeds 0.4 percent, and the burnup rate exceeds 3 percent per 10 000 hours.[2] Gas release is from the surface if there is no bubble motion or if either the fuel temperature is below 1225 K or the burnup is below 4 percent.

The bubble migration, interconnection, and surface release regions are shown pictorially on figure 5.

Discussion of Radioactive Gas Release

The diffusional transport-release equations derived in appendix B and used to correlate our online Kr^{88} release rate data only approximate the complex phenomena occurring inside fissioning fuel specimens. Not considered in the derivation are a broad range of interacting mechanisms; bubble nucleation, bubble growth, bubble coalescence, and gas resolution from bubbles. Nor have we examined bubble motion to determine

[2]These numbers are only approximations. They were obtained from the data in appendix E.

which of the bubble diffusion mechanisms (surface, volume, or gaseous) controls bubble velocity.

We have assumed that fission gas transport in UN by bubble diffusion is primarily dependent on fuel temperature and temperature gradient (as in eq. (B6)), and we have also assumed that the diffusion coefficients describing each of the three diffusion mechanisms (fission enhanced, atomic, and bubble) are additive in their effect on fission gas (as in eq. (B5)).

In effect, we have reduced a very complicated problem to a relatively simple one (eq. (1)) which very adequately describes the radioactive gas release rates from our fuel specimens, as shown in figure 2.

The Kr^{88} release rate data in figure 2 covers an activity range of from 3×10^{3} to 4×10^{6} disintegrations/cm^{3}-sec, and yet the average absolute relative difference

$$\frac{1}{n}\sum\left|\frac{A_{k,\,measured} - A_{k,\,calculated}}{A_{k,\,measured}}\right|$$

is only 13.8 percent. This 13.8 percent relative difference compares very favorably with the estimated uncertainties in activity measurements (±10 percent) and in the calculated fission rate densities (±15 to 20 percent).

Gas sample results for capsule 124 (table VII of appendix A) offer further verification of equation (1) which predicts that the release rate should be approximately proportional to $\lambda^{-1/2}$. For any two of the four isotopes measured (Kr^{85m}, K^{87}, Kr^{88}, or Xe^{135}) the relative activities in the sweep gas would be

$$\frac{\text{Activity}_1}{\text{Activity}_2} = \frac{Y_1}{Y_2}\left(\frac{\lambda_1}{\lambda_2}\right)^{1/2}\frac{e^{-\lambda_1 t_d}}{e^{-\lambda_2 t_d}}$$

where recoil has been neglected. Calculated and measured activity rates are compared in table III.

The best correlation obtained between our online Kr^{88} release rate data and equation (1) required that the bubble motion term

$$\left(\frac{\alpha_2 f e^{-Q_s/R_T}}{K_1^2 T^2}\right)$$

TABLE III. - COMPARISON OF CALCULATED AND MEASURED

ISOTOPIC ACTIVITY RATIOS

Isotope pair		Calculated activity ratio, activity$_1$/activity$_2$ if mechanism is -			Measured activity ratio	
1	2	$r \propto \left(\frac{1}{\lambda}\right)^{1/2}$	$r \propto \left(\frac{1}{\lambda}\right)$	$r \neq f(\lambda)$	Capsule 124[a]	Capsule 123[b]
Kr^{85m}	Kr^{87}	0.487	0.905	0.262	0.520	0.584
Kr^{85m}	Kr^{88}	.331	.418	.262	.349	.371
Kr^{88}	Kr^{87}	1.48	2.17	1.01	1.49	1.57
[c]Xe^{135}	Kr^{87}	1.91	5.07	.717	1.45	1.85

[a]Average of 26 gas samples for capsule 124 (table VII).

[b]Reported in ref. 5.

[c]Neglects neutron absorption in Xe^{135} and iodine decay to xenon outside fuel.

be set to zero for capsules 122 and 124. The postirradiation photomicrographs of capsules 122 and 124 (figs. 6 and 7) certainly do not show the large scale bubble formation and motion indicated in figure 1 for capsule 123. As indicated in table I, capsule 123 was operated to 1512 K while capsules 122 and 124 were only operated as high as 1225 and 1357 K, respectively.

Discussion of Stable Gas Release

The concept of fission gas release through interconnected grain boundary porosity is not new. It has been used by many authors to explain gas release and swelling behavior in nuclear fuels. Ainscough (ref. 8) shows how such intergranular porosity develops and interconnects in UO_2 fuel.

Our use of an interconnection model is primarily based on the evidence of postirradiation photomicrographs such as figures 1, 6, and 7. For one of our pins (capsule 122, fig. 6) there is little evidence of any intergranular porosity; for another (capsule 124, fig. 7) there appears to be some slight oriented porosity; and for another (capsule 123, fig. 1) there is extensive orientation and interconnection of intergranular porosity.

The maximum temperature at which each capsule operated increased from 1225 K for capsule 122 to 1357 K for capsule 124 to 1512 K for capsule 123 (table I). The higher the temperature of operation, the more intergranular porosity - at least for our fuel specimens which were operated to high burnups.

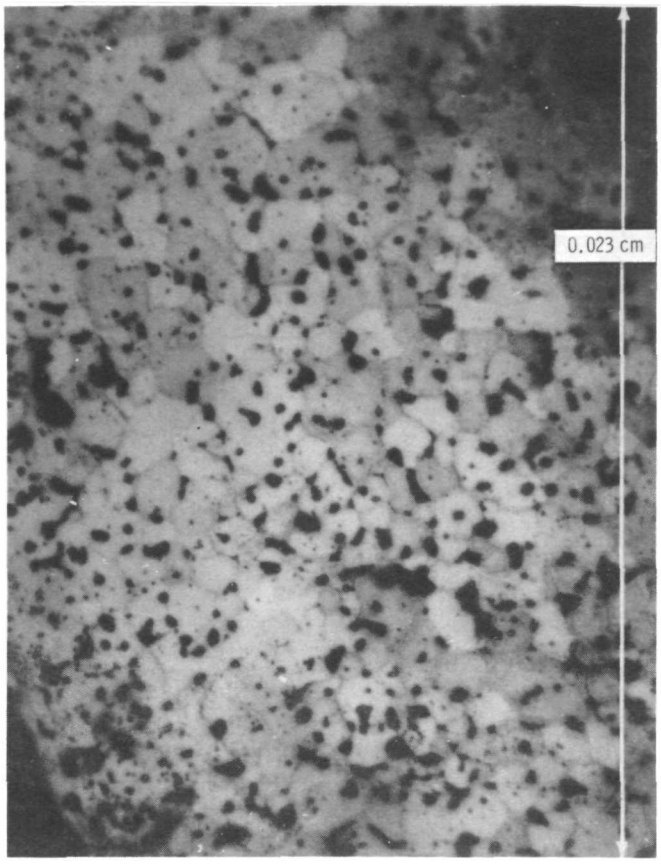

Figure 6. - Section of fuel pin in capsule 122. X500.

The actual derivation of the equations to predict stable gas release (as carried out in appendix D) contains a number of implicit and explicit assumptions. Our intent in the derivation was to include the important physical phenomena while obtaining relatively simple final relations for ease in interpretation and analysis.

Our basic assumptions are as follows:

(1) Fission gas release is to the grain boundaries. This is an obvious assumption for the ease where intergranular porosity exists and the intergranular space acts a sink. We assume no mechanism operates to get the gas back into the matrix. Resolution is neglected. When there is little intergranular porosity and little gas release, the diffusion or nondiffusion of gas across a grain boundary is umimportant. If gas could freely cross a boundary, then y_2 (the grain half-thickness in eq. (5)) would be replaced by the much larger dimension of half the fuel thickness and the calculated gas release would still be low.

(2) The intergranular gas pressure is at a constant pressure P (related to the gas

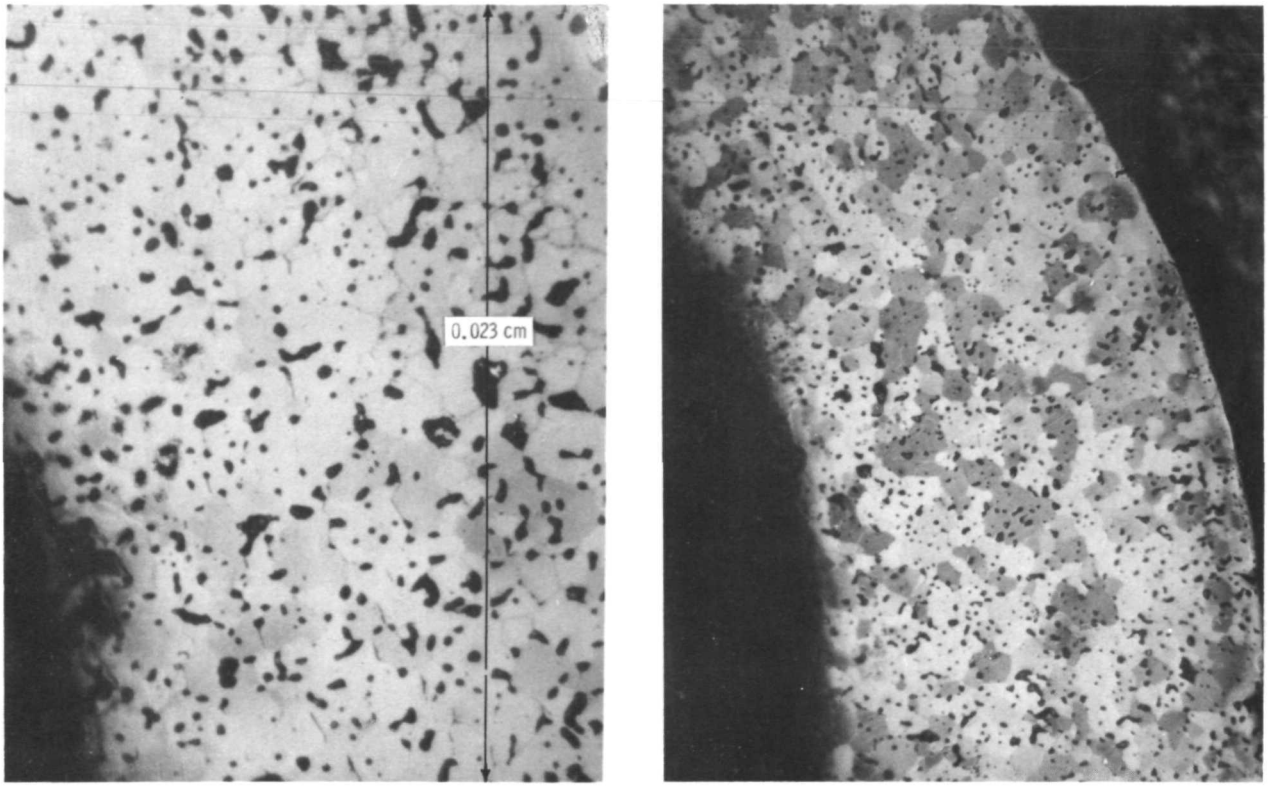

(a) X500. (b) X250.

Figure 7. - Section of fuel pin in capsule 124.

volume through the perfect gas law) and is assumed equal to the fuel-clad contact pressure.

(3) The fraction of intergranular porosity interconnected to the outside is directly porportional to the total intergranular porosity. Physically we would expect that the degree of interconnection would vary nonlinearly with porosity - starting out near zero until some critical porosity was reached - then increasing rapidly with additional gas volume - asymptotically approaching unity. A more complete description of this complex process, with various bubble sizes and velocities as well as competing gas transport processes would only becloud our analysis.

(4) All the porosity is intergranular. There is no simple way of distinguishing between inter and intragranular porosity as a time varient problem.

(5) A reasonable calculation of fuel-clad contact pressure can be made by assuming steady-state and equal tangential creep rates for the fuel and clad, proportional stresses in both the fuel and clad, and a very simplified fuel swelling rate.

The assumptions appear to work. As shown in figure 5 and table III, calculated and

measured gas releases agree very well - if bubble motion and interconnection are limited to definite temperature, burnup, and burnup rate regions as in figure 5. The minimum burnup limits shown in figure 6 do, in effect, add some nonlinearity to the porosity interconnection process, partially compensating for aforementioned assumption (3).

There are some inconsistancies in the basic gas release data used in our analyses and listed in table IX of appendix E. Comparisons of three of the tests (i.e., 6, 12, and 21) are shown in table IV.

TABLE IV. - INCONSISTENT GAS RELEASE DATA

Test designation	Fuel temperature, K	Time, hr	Burnup, percent	Measured R_T/B
12	1658	850	0.63	0.009
21	1665	1100	.74	.04
6	1533	1090	.42	.03
12	1658	850	.63	.009
21	1665	1100	.74	.04
6	1533	1090	.42	.03

In the first case (12 and 21), a factor of 5 difference in gas release is unjustified. In the second case (6 and 12), the much higher temperature has the lower gas release. In the third case (21 and 6), widely different temperatures result in similar releases.

We have no explanation for the inconsistent data. It is mentioned only to demonstrate a common problem in attempting to analyze fission gas release data.

SUMMARY OF RESULTS

A model has been developed to predict fission gas release from uranium nitride (UN) fuel pins clad with various materials. When correlated with measured gas releases from pins primarily clad with Nb-1Zr or PWC-11, operated to ~1650 K, the average deviation between calculated and measured gas release is 44 percent. The gas releases vary from 0.01 to 32 percent. If only the measured releases over 1 percent are considered, the average deviation is 26 percent.

In the model, fission gas is released to the grain boundaries where the porosity eventually interconnects and links to the outside. Interconnection does not take place if the fuel is below 1225 K or below 4 percent burnup. Bubble motion, one of the mech-

anisms for intragranular transport, exists only if the fuel temperature exceeds 1375 K, and the burnup exceeds 0.4 percent and the burnup rate exceeds 3 percent per 10 000 hours. Diffusion coefficients for the intragranular transport have been obtained from data measured in a sweep gas facility.

Fission gas release rates from UN specimens (sweep gas experiment data) irradiated to over 8 percent burnup at temperatures to 1789 K can be predicted to within 14 percent (mean absolute relative difference) where the release rate varies over three orders of magnitude. The standard deviation is 11 percent.

Lewis Research Center,
National Aeronautics and Space Administration,
Cleveland, Ohio, July 12, 1973,
503-05.

APPENDIX A

FISSION GAS RELEASE RATE DATA FOR UN FUEL SPECIMENS

Fission gas activities in the sweep gas were determined from online scintillation detector counts or film physical samples of the sweep gas which were analyzed by the Plum Brook Radiochemistry Section. Details of the procedures and the data for capsules 121, 122, and 123 have been previously presented in reference 5.

All of the online and gas sample Kr^{88} release rate data used to obtain values for the unknown constants in equation (1) are presented in tables V and VI.

Complete listings of the gas sample results for capsule 124, incomplete in time for inclusion in reference 5, are given in table VII.

TABLE V. - KRYPTON-88 ACTIVITY IN HELIUM SWEEP GAS

(a) Capsule 121

Experiment	Fuel maximum temperature, K	Fission-rate density, $\frac{\text{fissions}}{\text{cm}^3\text{-sec}}$	Fuel burnup, percent	Type of data[a]	K^{88} activity, $\frac{\text{disintegrations}}{\text{cm}^3\text{-sec}}$	
					Measured	Calculated[b]
1	1550	5.77×10^{14}	1.50	O	554×10^3	615×10^3
2	1550	5.77	1.83	O	720	664
3	1550	5.77	1.99	O	720	687
4	1550	5.77	2.23	O	860	723
5	1787	8.28	3.46	O	2810	2710
6	1787	8.28	5.06	O	3630	3420
7	1765	8.10	5.06	S	2560	3160
8	1778	8.18	6.03	O	3970	3710
9	1778	8.18	6.59	O	4240	3950
10	1765	8.10	6.65	S	3690	3810
11	1778	8.18	6.87	O	4380	4070
12	1218	3.34	8.07	O	215	228
13	1215	3.34	8.30	S	183	230
14	1218	3.34	8.77	O	263	243
15	1218	3.34	8.84	O	288	244
16	1218	3.34	8.93	O	285	246

[a]Sample, S; online, O.

[b]Value calculated using eq. (3).

TABLE V. - Continued. KRYPTON-88 ACTIVITY IN HELIUM SWEEP GAS

(b) Capsule 122

Experiment	Fuel maximum temperature, K	Fission-rate density, fissions / cm^3-sec	Fuel burnup, percent	Type of data[a]	K^{88} activity, disintegrations / cm^3-sec	
					Measured	Calculated[b]
1	1223	3.64×10^{14}	2.64	S	73.5	65.2×10^{3}
2	800	1.42	2.95	O	14.3	17.4
3	996	2.33	3.02	O	29.3	34.9
4	1219	3.59	3.09	O	68.7	69.2
5	598	.71	4.17	O	7.00	8.61
6	805	1.44	4.22	O	16.5	21.8
7	1002	2.37	4.31	O	34.3	43.8
8	1000	2.33	4.31	S	38.5	42.8
9	1223	3.65	4.40	O	86.8	87.2
10	1225	3.64	5.38	S	104	99.1
11	594	.692	5.40	O	9.30	9.82
12	804	1.44	5.44	O	26.9	25.6
13	1002	2.37	5.54	O	46.6	51.6
14	1223	3.65	5.64	O	102	103
15	598	.71	5.73	O	9.60	10.6
16	805	1.44	5.81	O	25.2	26.8
17	800	1.44	5.81	S	25.7	26.8
18	1000	2.33	5.93	S	57.2	52.7
19	1000	2.35	5.93	O	47.3	53.4
20	1220	3.60	6.03	S	101	105
21	598	.71	6.16	O	8.00	11.1
22	805	1.45	6.27	S	26.1	28.5
23	1227	3.64	6.59	S	118	114

[a]Sample, S; online, O.

[b]Value calculated using eq. (3).

TABLE V. - Continued. KRYPTON-88 ACTIVITY IN HELIUM SWEEP GAS

(c) Capsule 123

Experiment	Fuel maximum temperature, K	Fission-rate density, $\frac{\text{fissions}}{\text{cm}^3\text{-sec}}$	Fuel burnup, percent	Type of data[a]	K^{88} activity, $\frac{\text{disintegrations}}{cm^3\text{-sec}}$	
					Measured	Calculated[b]
1	585	0.505×10^{14}	1.51	O	3.85×10^{3}	3.33×10^{3}
2	795	1.10	1.54	O	9.65	9.07
3	795	1.10	1.54	S	10.7	9.07
4	990	1.83	1.60	O	23.7	20.1
5	1228	2.79	1.68	O	61.0	73.5
6	1387	3.60	1.78	O	152	197
7	1542	4.44	2.08	O	480	467
8	580	.496	3.57	O	5.35	4.87
9	580	.496	3.57	O	5.35	4.87
10	803	1.09	3.63	S	16.4	13.4
11	803	1.09	3.63	O	14.8	13.4
12	995	1.77	3.72	O	35.0	28.9
13	995	1.77	3.72	S	44.1	28.9
14	591	.505	4.33	O	4.30	5.57
15	591	.505	4.33	S	6.68	5.57
16	591	.505	4.33	O	5.00	5.57
17	804	1.09	4.39	O	17.0	15.1
18	804	1.09	4.39	S	22.0	15.1
19	1001	1.88	4.48	O	45.0	35.3
20	991	1.84	4.88	O	42.0	35.9
21	991	1.84	5.04	S	46.8	36.6
22	1222	2.77	5.19	O	130	129
23	1222	2.77	5.19	S	108	129
24	1380	3.56	5.39	O	350	343
25	1380	3.56	5.39	O	350	343
26	1541	4.44	5.86	O	950	836
27	1541	4.44	5.86	S	939	836
28	585	.505	5.87	O	6.40	6.82
29	995	1.77	5.92	O	45.0	38.8
30	1223	2.77	5.97	O	175	142
31	1390	3.62	6.04	O	470	393

[a]Sample, S; online, O.

[b]Value calculated using eq. (3).

TABLE V. - Concluded. KRYPTON-88 ACTIVITY IN HELIUM SWEEP GAS

(d) Capsule 124

Experiment	Fuel maximum temperature, K	Fission-rate density, $\frac{\text{fissions}}{\text{cm}^3\text{-sec}}$	Fuel burnup, percent	Type of data[a]	K^{88} activity, $\frac{\text{disintegrations}}{\text{cm}^3\text{-sec}}$	
					Measured	Calculated[b]
1	595	1.01×10^{14}	1.53	O	8.69×10^{3}	8.57×10^{3}
2	594	1.10	1.54	S	9.30	9.67
3	1002	3.81	1.84	O	53.2	56.3
4	1230	6.18	2.30	O	123	130
5	1230	6.18	2.38	O	148	132
6	808	2.25	2.58	O	29.2	31.3
7	810	2.35	2.58	S	29.2	33.3
8	425	.357	2.59	O	3.64	2.99
9	570	.904	2.66	O	11.4	9.45
10	480	.535	2.66	O	4.79	4.91
11	594	1.10	2.66	S	14.5	12.3
12	836	2.45	2.85	O	42.9	37.0
13	1306	7.28	3.33	O	212	208
14	1296	7.13	3.53	O	205	207
15	1294	7.12	3.53	S	193	206
16	1002	3.81	3.55	O	69.5	77.7
17	632	1.21	3.66	O	30.2	16.4
18	626	1.16	3.66	S	30.2	15.4
19	900	2.96	3.89	O	53.9	57.3
20	1316	7.45	4.48	O	252	258
21	1323	7.57	4.49	S	241	266
22	592	1.09	4.52	S	20.9	16.3
23	594	1.01	4.52	O	17.8	14.7
24	594	1.01	4.52	O	20.6	14.7
25	1003	3.82	4.87	O	97.1	94.5
26	1229	6.17	5.39	O	229	210
27	1232	6.33	5.40	S	202	218
28	439	.389	5.90	O	4.22	5.38
29	596	1.01	5.98	O	36.5	17.7
30	595	1.10	5.99	S	38.6	19.9
31	810	2.26	6.01	O	77.8	52.1
32	810	2.26	6.16	O	64.2	53.0
33	1016	4.13	6.48	S	109	128
34	1012	3.93	6.48	O	121	119
35	1226	6.14	7.53	O	229	263
36	1318	7.50	7.75	O	444	381
37	1318	7.51	7.76	S	454	382

[a]Sample, S; online, O.

[b]Value calculated using eq. (3).

TABLE VI. - KRYPTON-88 ACTIVITY IN NEON SWEEP GAS FOR CAPSULE 124

Experiment	Fuel maximum temperature, K	Fission-rate density, fissions/cm^3-sec	Fuel burnup, percent	Type of data[a]	K^{88} activity, disintegrations/cm^3-sec	
					Measured	Calculated[b]
1	849	1.01×10^{14}	1.59	O	12.0×10^3	11.3
2	851	1.07	1.60	S	10.7	12.1
3	999	1.55	1.64	O	19.9	18.8
4	1219	2.50	2.50	O	50.1	44.0
5	1219	2.49	2.51	S	54.4	43.8
6	429	.21	2.60	O	3.64	3.20
7	570	.39	2.61	O	5.33	5.34
8	595	.43	2.61	S	5.02	5.90
9	841	1.00	2.72	O	16.0	14.1
10	1219	2.50	2.90	O	74.2	47.3
11	1358	3.19	3.08	O	110	80.1
12	1363	3.15	3.10	S	113	79.9
13	629	.48	3.59	O	7.55	7.60
14	631	.50	3.60	S	7.39	8.04
15	895	1.18	3.72	O	19.5	20.2
16	1303	2.90	4.06	O	92.8	76.0
17	1308	2.88	4.06	S	105	75.8
18	833	.99	4.57	O	21.5	18.8
19	835	1.06	4.58	S	22.4	20.6
20	999	1.59	4.65	S	41.1	33.1
21	1000	1.55	4.65	O	36.9	32.0
22	1225	2.53	5.53	O	75.0	71.2
23	1221	2.50	5.54	S	81.8	70.0

[a]Sample, S; online, O.
[b]Value calculated using eq. (3).

TABLE VII. - FISSION GAS ACTIVITY FOR CAPSULE 124 (GAS SAMPLES)

(a) In helium sweep gas

Fuel maximum temperature, K	Fission-rate density, $\frac{\text{fissions}}{\text{cm}^3\text{-sec}}$	Fuel burnup, percent	Isotope activity, disintegrations/cm^3-sec			
			Kr^{85m}	Kr^{87}	Kr^{88}	Xe^{135}
806	2.33×10^{14}	0.53	7.96×10^{3}	18.2×10^{3}	25.2×10^{3}	22.2×10^{4}
803	2.29	.82	8.16	16.5	24.6	21.4
554	.90	.93	2.07	3.35	6.02	6.33
1008	3.99	1.42	19.6	39.3	56.5	48.3
594	1.10	1.54	3.23	5.93	9.30	8.96
810	2.35	2.58	10.0	19.0	29.2	28.5
594	1.10	2.66	5.02	8.95	14.5	14.7
1294	7.12	3.53	69.1	129	193	195
626	1.16	3.66	10.8	20.0	30.2	30.4
1323	7.57	4.49	87.9	162	241	238
592	1.09	4.52	7.62	14.2	20.9	20.3
1232	6.33	5.40	70.3	138	202	195
595	1.10	5.99	13.5	28.3	38.6	38.6
1016	4.13	6.48	38.1	71.6	109	103
1318	7.51	7.76	173	278	454	436

(b) In neon sweep gas

554	0.35×10^{14}	0.84	0.886×10^{3}	1.88×10^{3}	2.73×10^{3}	2.44×10^{3}
999	1.59	1.11	7.96	16.4	23.3	20.4
851	1.07	1.60	3.85	8.59	10.7	10.8
1219	2.49	2.51	19.8	36.4	54.4	57.6
595	.43	2.61	1.65	3.45	5.02	5.02
1363	3.15	3.10	40.5	75.5	113	128
631	.50	3.60	2.62	5.47	7.39	7.85
1308	2.88	4.06	35.5	67.9	105	107
835	1.06	4.58	7.85	15.0	22.4	23.7
999	1.59	4.65	14.9	27.5	41.1	43.2
1221	2.50	5.54	29.0	58.5	81.8	86.9

APPENDIX B

FUEL SPECIMEN FISSION GAS RELEASE RATE EQUATION

One-dimensional diffusion of a radioactive fission product gas through a fuel grain in a rectangular coordinate system can be described by the following equation:

$$\frac{\partial c}{\partial t} = D \frac{\partial^2 c}{\partial y^2} - \lambda c + fY \tag{B1}$$

where the diffusion coefficient D is assumed to be constant, and the fission-rate density f is independent of position in the fuel.

In steady state with $\partial c/\partial t = 0$ and with boundary conditions $\partial c/\partial y = 0$ at $y = 0$, and $c = 0$ at $y = y_1$, the solution of equation (B1) is

$$c(y) = \frac{fY}{\lambda}\left[1 - \frac{\cosh\left(\frac{\lambda}{D}\right)^{1/2} y}{\cosh\left(\frac{\lambda}{D}\right)^{1/2} y_1}\right] \tag{B2}$$

The fission gas release rate from the grain surface can be found by adding a direct recoil component (ref. 5) to the diffusional release, so that

$$R_g = \frac{PYSLf}{4} - DS \left.\frac{dc}{dy}\right|_{y_1} \tag{B3}$$

Differentiating equation (B2) and applying the result to equation (B3) gives

$$R_g = \frac{PYSLf}{4} + fYS\left(\frac{D}{\lambda}\right)^{1/2} \tanh\left(\frac{\lambda}{D}\right)^{1/2} y_1$$

which in turn reduces to

$$R_g = \frac{PYSLf}{4} + fYS\left(\frac{D}{\lambda}\right)^{1/2} \tag{B4}$$

$$\left(\frac{\lambda}{D}\right)^{1/2} y_1 >> 1$$

(which holds for all cases of practical interest).

If it is now assumed that there are three additive diffusion transport mechanisms (fission-enhanced diffusion, atomic diffusion, and pore migration) and furthermore that all pores have a constant velocity and diameter, D can be replaced by

$$D = D_{fo} f + D_o e^{-Q_o/RT} + v_p d_p \tag{B5}$$

Nichols in reference 2 shows that the velocity of a pore whose motion is controlled by surface diffusion can be given by (in his notation)

$$v_p = \left(\frac{2D_s V_s \Omega Q_s^*}{kT^2 r}\right)\left(\frac{3K}{2K + K'}\right)\nabla T_\infty \tag{B6}$$

where

D_s surface diffusion coefficient

V_s number of rate-controlling species per unit area

Ω molecular volume

Q_s^* surface heat of transport

k Boltzmann constant

T absolute temperature

r pore radius

K matrix thermal conductivity

K' pore thermal conductivity

∇T_∞ macroscopic temperature gradient

For our applications to cylindrical geometries we can replace equation (B6) first by

$$v_p d_p = \alpha_1 D_o e^{-Q_s/RT} \left(\frac{dT}{dy}\right) \frac{1}{T^2 K_1}$$

where α_1 is a constant, and then substitute dT/dr at the outer fuel radius for dT/dy where

$$\left.\frac{dT}{dr}\right|_{r_2} = \frac{2.75\times10^{-11} f r_2}{2K_1} \left(1 - \frac{r_1^2}{r_2^2}\right)$$

(fuel power in W/cu cm = 2.75×10^{-11}f) to get

$$R_g = \frac{pYSLf}{4} + \frac{fYS}{\lambda^{1/2}} \left(D_{fo} f + D_o e^{-Q_o/RT} + \alpha_2 e^{-Q_s/RT} \frac{f}{T^2 K_1^2}\right)^{1/2} \qquad \text{(B7)}$$

where

$$\alpha_2 = \frac{2.75\times10^{-11}}{2} r_2 \left(1 - \frac{r_1^2}{r_2^2}\right) \alpha_1 D_s$$

The recoil constant p is approximately proportional to gas density, so it may be approximated by α_3/T, where α_3 is a constant. As seen in reference 5, the experimental gas release rate data shows R_{pin} increasing linearly with burnup, so the final form of equation (B7) becomes

$$R_{pin} = (1 + \alpha_4 b) \left[\frac{\alpha_3 YSLf}{4T} + fYS \left(\frac{D_{fo} f + D_o e^{-Q_o/RT} + \frac{\alpha_2 f}{K_1^2 T^2} e^{-Q_s/RT}}{\lambda}\right)^{1/2}\right] \qquad \text{(B8)}$$

where $b > 1.5$ percent and s now refers to the total surface area through which gas is being released to the outside.

In our analysis we used the following simple relation between thermal conductivity K_1 and temperature T:

$$K_1(W/cm\text{-}K) = 0.1227 + 1\times10^{-4}T$$

APPENDIX C

NONLINEAR LEAST-SQUARES CORRELATION

The method of least squares can be applied to an equation nonlinear in terms of unknown constants. The procedure is presented in Scarborough (ref. 11) and is also outlined here.

(1) Assume you have an equation $y = f(x, a_1, a_2, a_3)$ which is nonlinear in the unknown constants a_1, a_2, and a_3, and a set of measured data points $(x_1, y_1), (x_2, y_2), \ldots, (x_n, y_n)$. Here y and x are general dependent and independent variables.

(2) Choose initial values for a_1, a_2, and a_3, such as a_{10}, a_{20}, and a_{30} where we would have

$$a_1 = a_{10} + \delta_1$$

$$a_2 = a_{20} + \delta_2$$

$$a_3 = a_{30} + \delta_3$$

when δ_1, δ_2, and δ_3 are unknown corrections. We are going to iteratively converge on values for a_1, a_2, and a_3 which minimize in a least-squares sense the differences between calculated and measured values of y.

(3) Expand the equation $y = f(x, a_1, a_2, a_3)$ about the initial values a_{10}, a_{20}, and a_{30} and retain only the first derivative terms so that, for each data set i,

$$y_i = f(x_i, a_{10}, a_{20}, a_{30}) + \delta_1\left(\frac{\partial f_i}{\partial a_1}\right) + \delta_2\left(\frac{\partial f_i}{\partial a_2}\right) + \delta_3\left(\frac{\partial f_i}{\partial a_3}\right)$$

(4) The "residual" equations of the following form:

$$v_i = y \text{ calc } i - y_i$$

are

$$v_i = \left[f(x_i, a_{10}, a_{20}, a_{30}) - y_i\right] + \delta_1\left(\frac{\partial f_i}{\partial a_1}\right) + \delta_2\left(\frac{\partial f_i}{\partial a_2}\right) + \delta_3\left(\frac{\partial f_i}{\partial a_3}\right) \qquad i = 1, N$$

For the method of least squares we want to minimize

$$g = \sum_{i=1}^{N} v_i^2 \tag{C1}$$

To do so, we obtain equations for $\partial g/\partial \delta_1$, $\partial g/\partial \delta_2$, and $\partial g/\partial \delta_3$ and set each equal to zero, and obtain three equations which can be solved for the unknown corrections δ_1, δ_2, and δ_3.

(5) Next, return to step (2) and obtain the following better values for the constants a_1, a_2, and a_3:

$$a_{11} = a_{10} + \delta_1$$

$$a_{21} = a_{20} + \delta_2$$

$$a_{31} = a_{30} + \delta_3$$

and repeat the entire process as often as needed until there are no significant changes in a_1, a_2, or a_3

The following equation (derived as eq. (B8)) was correlated with our Kr^{88} release rate data using this method:

$$R_{pin} = (1 + \alpha_4 b)\left[\frac{\alpha_3 YSLf}{4T} + fYS\left(\frac{D_{fo}f + D_o e^{-Q_o/RT} + \frac{\alpha_2 f}{K_1^2 T^2} e^{-Q_s/RT}}{\lambda}\right)^{1/2}\right] \tag{C2}$$

Values were obtained for the seven unknown constants α_4, α_3, D_{fo}, D_o, Q_o, α_2, and Q_s. Some specific steps are presented next.

To prevent computational problems, equation (C2) was scaled and rewritten as

$$\mathscr{A} = (1 + a_1 b)\left\{\frac{a_2 f'}{\mathscr{T}} + \left[a_3 f'^3 + a_4 f'^2 e^{23} e^{a_5/\mathscr{T}}\left(\frac{a_6 f' e^{a_7/\mathscr{T}}}{\mathscr{T}} + 1\right)\right]^{1/2}\right\} \tag{C3}$$

where the unknown constants are a_1 to a_7. $\mathscr{A}$, f', and $\mathscr{T}$ have been defined as

$$\mathscr{A} \triangleq \frac{\mathscr{A}_K}{10^3} = \frac{R_{pin} \lambda e^{-\lambda t_d}}{10^3}$$

$$f' \triangleq \frac{f}{10^{14}}$$

$$\mathscr{T} \triangleq \frac{T}{10^3}$$

Measured Kr^{88} activities vary over three orders of magnitude ($\sim 3\times10^3$ to $\sim 4\times10^6$ disintegrations/cm^3-sec), so in an effort to keep the higher activity data points from outweighing the lower activity points in the data fitting procedure, we minimized equations of the form

$$g = \sum \frac{v_i^2}{\mathscr{A}^2_{i,\,measured}}$$

instead of

$$g = \sum v_i^2$$

where

$$v_i = \mathscr{A}_{i,\,calculated} - \mathscr{A}_{i,\,measured}$$

In expanded form g is

$$g = \sum_{i=1}^{n} \left[\frac{(\mathscr{A}_{o,i} - \mathscr{A}_i) + \delta_1 \left(\frac{\partial \mathscr{A}_i}{\partial a_1}\right) + \delta_2 \left(\frac{\partial \mathscr{A}_i}{\partial a_2}\right) + \ldots + \delta_7 \left(\frac{\partial \mathscr{A}_i}{\partial a_7}\right)}{\mathscr{A}_{i,\text{measured}}} \right]^2$$

and the seven equations in the seven unknown corrections δ_i, which are found by setting $\partial g/\partial \delta_i = 0$, $i = 1, \ldots, 7$, are of the form

$$0 = \sum_{i=1}^{n} \left[\frac{\left(\frac{\partial \mathscr{A}_i}{\partial a_1}\right)(\mathscr{A}_{o,i} - \mathscr{A}_i) + \delta_1 \left(\frac{\partial \mathscr{A}_i}{\partial a_1}\right)^2 + \delta_2 \left(\frac{\partial \mathscr{A}_i}{\partial a_2}\right)\left(\frac{\partial \mathscr{A}_i}{\partial a_1}\right) + \ldots + \delta_7 \left(\frac{\partial \mathscr{A}_i}{\partial a_7}\right)\left(\frac{\partial \mathscr{A}_i}{\partial a_1}\right)}{\mathscr{A}^2_{i,\text{measured}}} \right]$$

Application of this fitting procedure to the data of table V of appendix A resulted in the equation

$$R_{pin} = (1 + 0.376b)\left\{ \frac{3.65\times10^{-3} Yf}{T} + fY\left[\frac{1.55\times10^{-29} f}{\lambda} + \frac{4.49\times10^{-9} e^{-\frac{18\,800}{T}}}{\lambda} + \frac{2.33\times10^{-16} f r_2}{T^2 K_1^2 \lambda}\left(1 - \frac{r_1^2}{r_2^2}\right) e^{-\frac{18\,400}{T}} \right]^{1/2} \right\}$$

APPENDIX D

STABLE GAS RELEASE FROM FUEL PIN

The extention of our previously developed fission gas release equations (appendix B) to describe the release of stable fission product isotopes from reactor-type fuel pins is accomplished in two steps. First equations relating gas release to intergranular porosity and intergranular gas pressure are developed and then the intergranular gas pressure is related to fuel and clad strength properties.

Porosity and Stable Gas Release

If it is assumed that the intergranular fission gas is at a constant pressure P, the rate of gas volume increase is given by the volume balance equation

$$\frac{dV_g}{dt} = R_g N_g \frac{KT}{P} - R_{ip} \frac{KT}{P} - R_s \frac{KT}{P} \tag{D1}$$

Then γ is defined as the fraction of intergranular gas volume connected to the fuel surface and so the release rate from interconnected porosity is represented by

$$R_{ip} = (R_g N_g - R_s)\gamma$$

so equation (D1) becomes

$$\frac{dV_g}{dt} = R_g N_g \frac{KT}{P} - (R_g N_g - R_s)\gamma \frac{KT}{P} - R_s \frac{KT}{P} \tag{D2}$$

Assume that γ is proportional to the intergranular porosity

$$\gamma = \beta \frac{V_g}{V_g + V_f} \tag{D3}$$

where the coefficient β governs the rapidity at which interconnection occurs. As an approximation

$$\gamma = \beta \frac{V_g}{V_f}$$

and equation (D2) then becomes

$$\frac{dV_g}{dt} = (R_g N_g - R_s) \frac{KT}{P} - (R_g N_g - R_s) \beta \frac{V_g}{V_f} \frac{KT}{P}$$

or

$$dV_g + \frac{(R_g N_g - R_s)}{V_f} \frac{KT}{P} \beta V_g \, dt = (R_g N_g - R_s) \frac{KT}{P} dt$$

The solution to this linear first-order equation is (ref. 12)

$$V_g \exp\left[\int (R_g N_g - R_s) \frac{KT\beta}{PV_f} dt\right] = \left(\int \left[(R_g N_g - R_s) \frac{KT}{P}\right] \times \left\{\exp\left[\int (R_g N_g - R_s) \frac{KT\beta}{PV_f} dt\right] dt\right\}\right) + \text{constant} \qquad \text{(D4)}$$

The integration

$$\int (R_g N_g - R_s) \frac{KT\beta}{PV_f} dt$$

in equation (D4) can be performed if we have both R_g and R_s as functions of t. In our previous report (ref. 5) we showed that the diffusional release from a rectangular grain (neglecting surface recoil) is

$$R_g = fYy_2S\left(1 - \frac{8}{\pi^2}\sum_{n=0}^{\infty}\frac{\exp\left\{-D\left[\frac{(2n+1)}{2}\frac{\pi}{y_2}\right]^2 t\right\}}{(2n+1)^2}\right) \tag{D5}$$

For values of $D\pi^2 t/4y_2^2 \leq 1$ [3] equation (D5) can be approximated by

$$R_g = 0.718\, fYy_2S\left(\frac{D\pi^2 t}{4y_2^2}\right)^{1/2}$$

or

$$R_g = 0.359\, fYV_g\,\frac{D\pi^2}{4y_2^2}\,t = dt^{1/2}$$

if we also assume that

$$R_s = FR_gN_g = FCN_g\,t^{1/2}$$

equation (D4) becomes

$$V_g \exp\left[\int (1 - F)dN_g\, t^{1/2}\,\frac{KT\beta}{PV_f}\,dt\right] = \left(\int\left[(1 - F)dN_g\, t^{1/2}\,\frac{KT}{P}\right]\right.$$

$$\left.\times\left\{\exp\left[\int (1 - F)dN_g\, t^{1/2}\,\frac{KT\beta}{PV_f}\,dt\right]dt\right\}\right) + \text{constant}$$

[3] This corresponds to an instantaneous release to birth rate of less than 70 percent.

which yields

$$V_g \exp\left[\frac{2}{3}\frac{KT\beta(1-F)dN_g}{PV_f}t^{3/2}\right] = \left(\int\left[(1-F)dN_g\, t^{1/2}\frac{KT}{P}\right] \times\left\{\exp\left[\frac{2KT\beta(1-F)dN_g}{3PV_f}t^{3/2}\right]dt\right\}\right) + \text{constant}$$

If we remove V_f/β from the integral on the right, it becomes of the form $\int u'e^{\delta u}\,dt$ with solution $1/\delta e^{\delta u}$. Thus the solution becomes

$$V_g \exp\left[\frac{2}{3}\frac{KT\beta(1-F)dN_g\, t^{3/2}}{PV_f}\right] = \frac{V_f}{\beta}\exp\left[\frac{2}{3}\frac{KT\beta(1-F)dN_g\, t^{3/2}}{PV_f}\right] + \text{constant}$$

or

$$V_g = \frac{V_f}{\beta}\left\{1 + h\exp\left[-\frac{2}{3}\frac{KT\beta(1-F)dN_g\, t^{3/2}}{PV_f}\right]\right\}$$

The constant h can be determined from the initial condition $V_g = V_{g_0}$ at $t = 0$. Then

$$V_g = \frac{V_f}{\beta}\left\{1 + \left(\frac{V_{g_0}\beta}{V_f} - 1\right)\exp\left[-\frac{2KT\beta(1-F)dN_g\, t^{3/2}}{3PV_f}\right]\right\} \qquad \text{(D6)}$$

The fission gas release rate from a fuel pin can now be calculated as follows:

$$R_{pin} = R_{ip} + R_s = (R_g N_g - R_s)\gamma + R_s = (R_g N_g - R_s)\frac{\beta V_g}{V_f} + R_s$$

Using equation (D6) and $R_s = FN_g R_g$ we get

$$R_{pin} = (1 - F)R_g N_g \left(1 + \left(\frac{V_{g_0}\beta}{V_f} - 1\right)\left\{\exp\left[-\frac{2KT\beta(1 - F)dN_g\, t^{3/2}}{3PV_f}\right]\right\}\right) + FR_g N_g \qquad \text{(D7)}$$

If we rearrange equation (D7) and replace R_g by $dt^{1/2}$, we can integrate to get the total gas release from a pin

$$R_{T,pin} = \frac{2}{3}dN_g\, t^{3/2} + (1 - F)N_g\, d\left(\frac{V_{g_0}\beta}{V_f} - 1\right)\int_0^t \left\{t^{1/2}\exp\left[-\frac{2}{3}\frac{KT\beta(1 - F)dN_g\, t^{3/2}}{PV_f}\right]dt\right\}$$

$$R_{T,pin} = \frac{2}{3}dN_g\, t^{3/2} + \frac{2}{3}\frac{PV_f\left(\frac{V_{g_0}\beta}{V_f} - 1\right)}{KT\beta}\left\{1 - \exp\left[-\frac{2}{3}\frac{KT\beta(1 - F)dN_g\, t^{3/2}}{PV_f}\right]\right\} \qquad \text{(D8)}$$

Equation (D8) can be put into terms of total release to total birth by dividing by $fYV_f t$ to give

$$\frac{R_T}{B} = \frac{\frac{2}{3}dN_g\, t^{3/2}}{fYV_f t} + \frac{2PV_f\left(\frac{V_{g_0}\beta}{V_f} - 1\right)}{3KT\beta fYV_f t}\left\{1 - \exp\left[-\frac{2}{3}\frac{KT\beta(1 - F)dN_g\, t^{3/2}}{PV_f}\right]\right\} \qquad \text{(D9)}$$

Since the total release from a grain is given by

$$\int_0^t R_g \, dt = d \int_0^t t^{1/2} \, dt = \frac{2}{3} dt^{3/2}$$

and the total birth in a grain is $fYV_g t$, equation (D9) becomes

$$\frac{R_T}{B} = \left(\frac{R_T}{B}\right)_g + \frac{2P\left(\frac{V_{g_0}\beta}{V_f} - 1\right)}{3KT\beta fYt} \left\{1 - \exp\left[-\frac{KT\beta(1 - F)fYt}{P}\left(\frac{R_T}{B}\right)_g\right]\right\}$$

For a cylindrical fuel pin with an outside radius r_2 and an inside radius r_1, $F = 2y_2/(r_2 - r_1)$ and the final form of the release equation becomes

$$\frac{R_T}{B} = \left(\frac{R_T}{B}\right)_g - \frac{2P\left(1 - \frac{V_{g_0}\beta}{V_f}\right)}{3KT\beta fYt} \left\{1 - \exp\left[-\frac{KT\beta fYt\left(1 - \frac{2y2}{r_2 - r_1}\right)}{P}\left(\frac{R_T}{B}\right)_g\right]\right\} \qquad \text{(D10)}$$

In doing the calculations with equation (D10), the quotient V_{g_0}/V_f is considered to be the initial fuel porosity and $(R_T/B)_g$ is calculated from the integrated form of equation (D5), not the approximate form $R_g = dt^{1/2}$.

Fuel-Clad Contact Pressure

The tangential creep rate (fuel or clad) is given by (ref. 13)

$$\dot{\epsilon}_\theta = \frac{\dot{\epsilon}_e}{2\sigma_e}(2\sigma_\theta - \sigma_r - \sigma_z) \qquad \text{(D11)}$$

Assume that the steady-state equivalent strain rate and equivalent stress are related by

$$\dot{\epsilon}_e = A\sigma_e^n$$

where A is a function of temperature. Equation (D11) becomes

$$\dot{\epsilon}_\theta = \frac{A}{2}\sigma_e^{n-1}(2\sigma_\theta - \sigma_r - \sigma_z) \tag{D12}$$

The equivalent stress σ_e can be written as

$$\sigma_e = \frac{1}{\sqrt{2}}\left[(\sigma_r - \sigma_\theta)^2 + (\sigma_\theta - \sigma_z)^2 + (\sigma_z - \sigma_r)^2\right]^{1/2}$$

and if we assume the following proportional stresses:

$$\sigma_\theta = k_1\sigma_r \tag{D13}$$

$$\sigma_z = k_2\sigma_r \tag{D14}$$

then σ_e becomes

$$\sigma_e = \frac{1}{\sqrt{2}}\left\{\sigma_r^2\left[(1 - k_1)^2 + (k_1 - k_2)^2 + (k_2 - 1)^2\right]\right\}^{1/2} = k_3|\sigma_r| \tag{D15}$$

where k_3 is a constant. Combining equations (D12) and (D15) yields

$$\dot{\epsilon}_\theta = k_4|\sigma_r|^{(n-1)}\sigma_r A \tag{D16}$$

where

$$k_4 = \frac{1}{2}k_3^{(n-1)}(2k_1 - k_2 - 1)$$

If we now equate fuel and clad tangential creep rates

$$\dot{\epsilon}_{\theta c} = \dot{\epsilon}_{\theta f} + \frac{1}{3}\dot{v}$$

where $\dot{v}$ is the fuel bulk strain rate, and substitute for $\dot{\epsilon}_\theta$ using equation (D16), we get

$$A_c k_{4c} |\sigma_{rc}|^{(n_c-1)} \sigma_{rc} = A_f k_{4f} |\sigma_{rf}|^{(n_f-1)} \sigma_{rf} + \frac{1}{3}\dot{v} \tag{D17}$$

At the interface we equate the radial stresses and fuel-clad contact pressure $\sigma_r = -P$, and equation (D17), after rearranging, becomes

$$P^{(n_c-n_f)} = \frac{A_f k_{4f}}{A_c k_{4c}} - \frac{1}{3}\frac{\dot{v}}{k_{4c} A_c P^{n_f}} \tag{D18}$$

To use equation (D18), values for k_4 and $\dot{v}$ have to be found.

The constant k_1, defined by equation (D13), can be approximated using the equations for stress in thick-walled cylinders (ref. 14)

$$\sigma_r = \frac{1}{c^2 - a^2}\left[a^2 P_i - C^2 P_o - \left(\frac{ac}{r}\right)^2 (P_i - P_o)\right] \tag{D19}$$

$$\sigma_\theta = \frac{1}{c^2 - a^2}\left[a^2 P_i - C^2 P_o + \left(\frac{ac}{r}\right)^2 (P_i - P_o)\right] \tag{D20}$$

where c is the external radius and a is the internal radius.

For the fuel, equations (D19) and (D20) are evaluated at the fuel outside radius r_2 with $P_o = 0$, giving

$$k_{1f} = \frac{\left(r_1^2 + r_2^2\right)}{\left(r_2^2 - r_1^2\right)} \tag{D21}$$

and for the clad, equations (D19) and (D20) are evaluated at the clad inside radius with $P_i = 0$, yielding

$$k_{1c} = \frac{\left(r_3^2 + r_2^2\right)}{\left(r_3^2 - r_2^2\right)} \tag{D22}$$

Then k_2, defined by equation (D14), can be approximated by an elastic calculation - assuming that the fuel and the clad do not slip.

In the axial direction

$$\epsilon_z = \frac{1}{E}\left[\sigma_z - r(\sigma_\theta + \sigma_r)\right]$$

and since $\epsilon_{zc} = \epsilon_{zf}$

$$\frac{\sigma_{zc}}{E_c} - \frac{\sigma_{zf}}{E_f} = -\frac{1}{E_f}\left[V_F(\sigma_{\theta f} + \sigma_{rf})\right] + \frac{1}{E_c}\left[V_c(\sigma_{\theta c} + \sigma_{rc})\right]$$

The forces creating σ_{zc} and σ_{zf} are equal and opposite, so

$$\frac{\mathscr{F}_z}{S_c E_c} + \frac{\mathscr{F}_z}{S_f E_f} = \frac{V_c}{E_c}(\sigma_{\theta c} + \sigma_{rc}) - \frac{V_f}{E_f}(\sigma_{\theta f} + \sigma_{rf}) \qquad \text{(D23)}$$

where S_f and S_c are the cross-sectional areas of the fuel and clad and $\mathscr{F}$ is the force.

Evaluating equation (D13) at the fuel-clad interface where

$$\sigma_{rf} = -P_o$$

$$\sigma_{rc} = -P_i$$

$$\sigma_{\theta f} = -\frac{\left(r_2^2 + r_1^2\right)}{\left(r_2^2 - r_1^2\right)} P_o$$

$$\sigma_{\theta c} = \frac{\left(r_3^2 + r_2^2\right)}{\left(r_3^2 - r_2^2\right)} P_i$$

yields

$$\mathscr{F}_z = \frac{\left[\frac{V_c}{E_c}\left(\frac{r_3^2 + r_2^2}{r_3^2 - r_2^2} - 1\right) + \frac{V_f}{E_f}\left(\frac{r_2^2 + r_1^2}{r_2^2 - r_1^2} + 1\right)\right] P}{\left(\frac{1}{S_c E_c} + \frac{1}{S_f E_f}\right)} \tag{D24}$$

and since $\sigma_{zc} = \mathscr{F}_z/S_c$ and $\sigma_{zf} = \mathscr{F}_z/S_f$, we obtain from equation (D24)

$$k_{2c} = \frac{-\left[\frac{V_c}{E_c}\left(\frac{r_3^2 + r_2^2}{r_3^2 - r_2^2} - 1\right) + \frac{V_f}{E_f}\left(\frac{r_2^2 + r_1^2}{r_2^2 - r_1^2} + 1\right)\right]}{\left(\frac{1}{E_c} + \frac{S_c}{E_f S_f}\right)} \tag{D25}$$

$$k_{2f} = -\frac{k_{2c} S_c}{S_f} \tag{D26}$$

Then k_4 can be calculated from k_1 and k_2, since

$$k_4 = \frac{1}{2} k_3^{(n-1)} (2k_1 - k_2 - 1)$$

and

$$k_3 = \frac{1}{\sqrt{2}}\left[(1 - k_1)^2 + (k_1 - k_2)^2 + (k_2 - 1)^2\right]^{1/2}$$

An approximation to the fuel bulk strain rate $\dot{v}$ can be obtained by considering the fuel swelling to be unrestrained. Lietzke (ref. 10) obtained integral equations for unrestrained swelling and has presented the results graphically with $\dot{v}\tau$ plotted as a

function of a dimensionless parameter Π [4] for various values of the fuel creep rate stress exponent n_f.

Two simple empirical approximations to the integral equation result for $\dot{v}\tau$ are

$$\dot{v}\tau = 6.5\left(n_f + 3\right)^{0.285}\Pi^{(n_f+3)/n_f} \qquad \begin{cases} n_f \geq 3, \ \Pi \geq 0.1, \text{ or} \\ n_f \geq 4, \ \Pi \geq 0.04, \text{ or} \\ n_f \geq 5, \ \Pi \geq 0.02, \text{ or} \\ n_f > 6 \end{cases} \tag{D27}$$

and

$$\dot{v}\tau = 2\,\frac{n_f - 1}{n_f}\left(n_f - 1\right)^{1/n_f}\Pi^{(n_f+1)/n_f} \qquad \begin{cases} n_f < 3, \ \Pi < 0.1, \text{ or} \\ n_f < 4, \ \Pi < 0.04, \text{ or} \\ n_f < 5, \ \Pi < 0.02, \text{ or} \\ n_f < 6 \end{cases} \tag{D28}$$

Comparisons of the simplified relations with the integral solution are shown in table VIII.

4

$$\Pi = \left[\frac{3A\tau}{2(n_f + 1)}\right]^{1/(n_f+1)}\left(\frac{3CyKTNB}{n_f}\right)^{n_f/(n_f+1)}$$

where in Lietzke's notation τ is test time, B is fractional burnup, N is fissionable atom density, and CY is fraction of gaseous fission products.

TABLE VIII. - UNRESTRAINED FUEL SWELLING

[Comparison of approximate and integral solution for $\dot{v}_T$.]

n_f	π	0.01	0.02	0.04	0.06	0.08	0.10	0.12
3	$\dot{v}_T$ integral	----	0.01	0.027	0.050	0.080	0.117	0.160
	$\dot{v}_T$ approx.	----	.014	.035	.059	.087	.108	.156
4	$\dot{v}_T$ integral	----	.016	.044	.083	.136	.201	.28
	$\dot{v}_T$ approx.	----	.019	.040	.082	.136	.201	.28
5	$\dot{v}_T$ integral	0.01	.023	.064	.122	.205	.295	>.33
	$\dot{v}_T$ approx.	.01	.022	.068	.130	.207	.295	>.33
6	$\dot{v}_T$ integral	.012	.031	.087	.175	.295	>.33	-----
	$\dot{v}_T$ approx.	.012	.034	.097	.179	.275	>.33	-----
7	$\dot{v}_T$ integral	.015	.039	.115	.23	>.33	-----	-----
	$\dot{v}_T$ approx.	.017	.047	.126	.23	-----	-----	-----

APPENDIX E

STABLE GAS RELEASE DATA FROM UN FUEL PINS

All of the stable gas release data used to correlate with the equations developed in appendix D are presented in this section. The data comes from various sources (refs. 15 to 19) and describes gas releases from pins clad with T-111, Nb-1Zr, PWC-11, and W-26Re irradiated at temperatures ranging from 1100 to 1900 K.

Grain sizes for most of the pins listed in table IX were estimated from photomicrographs of fuel in similar capsules.

Materials properties for the various clad materials along with the values used for UN are given in table X.

TABLE IX. - STABLE GAS RELEASE DATA

Experiment	Test description	Fuel code[a]	Clad code[b]	Fuel temperature, K	Clad temperature, K	Time, hr	Grain size, cm	Measured R/B	Clad outside radius, cm	Clad inside radius, cm	Fuel inside radius, cm	Initial porosity	Fission-rate density, fissions cm^3-sec	Burnup, percent
1	PW26-200 42	2	4	1144	1103	390	0.00330	0.0008	0.3985	0.3100	0	0.096	0 1600E+14	0.060
2	PW26-200 43			1248	1214	390		.0009				.090	.1490E+14	060
3	PW26-201 40			1443	1353	1 590		.0350				092	.3530E+14	570
4	PW26-201 41			1422	1311	1 590		0510				.097	.4470E+14	720
5	PW26-210 108			1477	1380	1 090		.0300	3925	.3035		.039	.4040E+14	.420
6	PW26-210 109			1533	1436	1 090		.0330				.039	.4070E+14	420
7	PW26-210 110			1533	1436	1 090		.0250				038	.3820E+14	.400
8	PW26-220 118			1429	1297	1 690		.0480				.059	.5600E+14	1.200
9	PW26-220 119			1582	1450	1 690		.1170				.057	.5560E+14	1.200
10	PW26-220 120			1443	1297	1 690		.0420				.060	.5640E+14	1.210
11	PW26-230 123			1568	1408	850		0053	3960	.3075		.056	.6620E+14	.580
12	PW26-230 124			1658	1492	850		.0088				.040	.7090E+14	.630
13	PW26-230 125			1547	1380	850		0068				043	.6910E+14	.610
14	PW26-231 126			1533	1353	2 750		0990				.040	.7820E+14	2.260
15	PW26-231 127			1665	1492	2 750		.2910				039	.7710E+14	2.230
16	PW26-231 128			1581	1394	2 750		.1110				038	.8070E+14	2 340
17	PW26-240 132			1554	1408	3 000		.1720		3125		.050	5820E+14	1.650
18	PW26-240 133			1637	1478	3 000		.3230				.051	.6550E+14	1.820
19	PW26-240 134			1568	1436	3 000		2190				056	.5460E+14	1 510
20	PW26-241 135			1616	1436	1 100		0580				051	.7490E+14	.780
21	PW26-241 136			1665	1492	1 100		.0390				.053	.7270E+14	740
22	PW26-241 137			1588	1422	1 100		.0400				.057	.6980E+14	.720
23	PW600 TOP			1348	1313	662		.0010	3175	.2415		.022	.1960E+14	.190
24	PW600 MID			1470	1438	662						.039	1960E+14	.180
25	PW600 BOT			1483	1448	662						.045	.1930E+14	.180
26	PW601 TOP			1403	1368	1 372						.033	1710E+14	.390
27	PW601 MID			1470	1438	1 372		.0020				.038	.1750E+14	.390
28	PW601 BOT			1458	1423	1 372		0020				.044	.1750E+14	400
29	PW603 TOP			1265	1218	3 310		0005				.038	2470E+14	.780
30	PW603 MID			1408	1368	3 310		0010				.042	.2400E+14	760
31	PW603 BOT			1388*	1338	3 310		0006				.045	.2470E+14	.780
32	ORNL612 TOP		5	1240	1143	5 205	.00290	0005				.043	.4290E+14	2.540
33	ORNL612 MID			1350	1248	5 250		0037					.4290E+14	2.540
34	ORNL612 BOT			1285	1188	5 205		0009					.4290E+14	2.540
35	ORNL642			1475	1453	9 966		0034					.1050E+14	1.180
36	ORNL649			1460	1433	10 512		.0004					.1240E+14	1.430
37	ORNL652 MID			1543	1478	3 180		.0009					.1960E+14	.700
38	ORNL656 TOP			1538				.0003					.1800E+14	.600
39	ORNL656 MID			1538				.0011					.1800E+14	.600
40	ORNL656 BOT			1538				.0013					1600E+14	.600
41	ORNL658 MID			1480	1458	9 779		.0014					.9820E+13	1.080
42	ORNL658 BOT			1460	1438	9 779		.0009					.9820E+13	1.080
43	ORNL660 MID			1558	1478	2 635		0005					.2320E+14	.070
44	ORNL662 TOP			1363	1338	10 270		.0001					1130E+14	1.160
45	ORNL662 MID			1498	1473	10 270		0008					1130E+14	1.160
46	ORNL662 BOT			1488	1463	10 270		0004					.1130E+14	1.160
47	ORNL665 TOP			1228	1133	9 583		0136					.4220E+14	4.580
48	ORNL665 MID			1332	1238	9 583		.0596					.4220E+14	4.580
49	ORNL665 BOT			1275	1178	9 583		0178					.4220E+14	4.580
50	ORNL667 MID			1473	1448	6 209		0002					1090E+14	780
51	ORNL667 BOT			1478	1453	6 209		.0003					.1090E+14	.780
52	ORNL669 TOP			1160	1108	10 352		.0005					.2330E+14	2.720
53	ORNL669 MID			1300	1253	10 352		.0013					.2330E+14	2.720
54	ORNL669 BOT			1255	1203	10 352		.0012					.2330E+14	2.720
55	ORNL002 3FMT			1497	1476	10 173		.0006					.9820E+13	1 120
56	ORNL003 TOP			1443	1373	11 985		.0600					.3090E+14	4.170
57	ORNL003 2FMT			1503	1433			.1030						
58	ORNL003 3FMT			1528	1458			.1150						
59	ORNL003 BOT			1503	1433			.1260						
60	ORNL UN1 TOP		7	1393	1313	8 250	.00293	.0014	.9271	.7747	.2667	.060	.1850E+14	1.780
61	ORNL UN3 TOP		7	1598	1573	5 807	.00293	.0010	.9271	.7747	.2667	.060	.2350E+14	1.450
62	ORNL UN3 BOT		3	1920	1673	5 807	.00293	.0710	.9271	.7747	0	.055	.2850E+14	1.750
63	NASA 504B			1255	1255	8 070	.00300	.0005	9110	.7950	.2550	.060	.5050E+13	.470
64	NASA 503B			1270	1255	8 070	.00300	0010	.4580	.3980	.1420	051	.9560E+13	.890
65	NASA 503C			1271	1255	8 070	.00300	0010	.4580	.3980	.1420	.051	.9840E+13	.920

[a]Fuel code 2 refers to UN with oxygen content over 1000 ppm.

[b]Clad code 4: Nb-1Zr

Clad code 5: PWC-11 (Nb-1 wt. % Zr-0 1 wt % C)

Clad code 7: T-111 (Ta-8 wt. % W-2 wt. % Hf)

Clad code 3 W-26Re (or W-25Re)

TABLE X. - MATERIALS PROPERTIES

Material	Property	Source
	Elastic modulus	
UN	$E = \left(38.7\times10^{6} - 100.5\times10^{6}\,\frac{V_g}{V_f}\right)[1 - 6.16\times10^{-5}(T - 77)]$	Refs. 20 and 21
Nb-1Zr	$E = 11.8\times10^{6} - 3667\,T$	Ref. 22
PWC-11	Assumed same as Nb-1Zr	----------
T-111	$E = 26.1\times10^{6} - 1700\,T$	Ref. 23
W-26Re	$E = 62.8\times10^{6} - 4667\,T$	Private communication from I. Fiero, NASA Lewis Research Center
	Poisson s ratio	
UN	$\gamma = 0.284 - 0.382\,\frac{V_g}{V_f}$	Ref. 20
T-111	$\gamma = 0.25$	Unpublished TRW data obtained from I. Fiero, NASA Lewis Research Center
Others	$\gamma = 0.30$	----------
	Creep rate constants $\dot{\epsilon}_e(hr^{-1}) = a_1 e^{-a_2/T(K)}\,\sigma_e(N/cm^2)^n$	
UN	$\dot{\epsilon}_e = 3.88\times10^{-11}\,e^{-31\,088/T}\,\sigma_e^{4.661}$	Ref. 24
Nb-1Zr	$\dot{\epsilon}_e = 3.88\times10^{-11}\,e^{-44\,604/T}\,\sigma_e^{5.988}$	Ref. 25
PWC-11	$\dot{\epsilon}_e = 5.717\times10^{-15}\,e^{-42\,700/T}\,\sigma_e^{5.988}$	Private communication from R. L. Smith, NASA Lewis Research Center
T-111	$\dot{\epsilon}_e = 2.214\times10^{-5}\,e^{-47\,776/T}\,\sigma_e^{3.692}$	Ref. 25
W-26Re	$\dot{\epsilon}_e = 5.95\times10^{-5}\,e^{-45\,676/T}\,\sigma_e^{3.377}$	Private communication from W. F. Mattson, NASA Lewis Research Center

APPENDIX F

SYMBOLS

A	creep rate constant
A_k	activity of Kr^{88} in sweep gas, disintegrations/cm^3-sec
$\mathscr{A}$	activity/10^3
a_i	constants (i = 1, 2, . . . , 7)
B	total birth (atoms formed by fission), atoms
b	burnup, percent uranium atoms fissioned
c	fission gas concentration, atoms/cm^3
D	total diffusion coefficient, cm^2/sec
D_{fo}	fission-enhanced diffusion constant, cm^5/fission
D_o	atomic diffusion constant, cm^2/sec
D_s	surface diffusion constant, cm^2/sec
d	combination of terms: $0.359\ fYV_g D\pi^2/4y_2^2$
d_p	pore diameter, cm
E	elastic modulus
F	constant, fraction of fission gas released from surface
$\mathscr{F}$	axial force
f	fission-rate density, fissions/cm^3-sec
f'	$f/10^{14}$
g	sum defined by eq. (C1)
h	constant
K	gas constant, 1.381×10^{-21} N-cm/molecule-K
K_1	thermal conductivity, W/cm-K
k_i	stress proportionality constants (i = 1, 2, 3)
k_4	constant
L	recoil length in fuel, cm
N_g	number of grains

n	creep rate equation stress exponent
P	pressure
p	fraction of recoils stopped by gas after ejection
Q_o	energy of activation for atomic diffusion, J/mole
Q_s	energy of activation for surface diffusion, J/mole
R	gas constant, 8.314 J/mole-K
R_g	release rate from grain, atoms/sec
R_{ip}	release rate from interconnected porosity, atoms/sec
R_{pin}	release rate from a fuel pin, atoms/sec
R_s	release rate from the fuel surface, atoms/sec
R_T	total gas release, atoms
r_1	fuel inside radius, cm
r_2	fuel outside radius or clad inside radius, cm
r_3	clad outside radius, cm
S	fuel surface area, cm^2
T	temperature, K
$\mathcal{T}$	temperature/10^3
t	time, sec
t_d	decay time in sweep gas, sec
u	function of t
V_f	volume of fuel, cm^3
V_g	volume of intergranular gas, cm^3
V_{g_0}	initial volume of intergranular gas, cm^3
$\dot{v}$	fuel bulk strain rate
v_i	difference between calculated and measured values for i^{th} data set
v_p	pore velocity, cm/sec
Y	fission yield, atoms/fission
y	coordinate distance, cm
y_1	thickness, cm

y_2 half thickness, cm

α_1 constants

β proportionality constant, $\gamma = \beta V_g/(V_g + V_f)$

γ fraction of intergranular volume connected to fuel surface

δ constant

δ_1 correction factors in Taylor expansion

$\dot{\epsilon}$ creep rate

λ decay constant, sec^{-1}

ν Poisson's ratio

π dimensionless parameter

σ stress

τ test time

Subscripts:

c clad

e equivalent

f fuel

i internal

o external

r coordinate direction

z coordinate direction

θ coordinate direction

REFERENCES

1. Carroll, R. M.: Fission-Gas Effects in Reactor Fuels - Part I. Basic Studies. Nucl. Safety, vol. 12, no. 4, July-Aug. 1971, pp. 297-305.
2. Nichols, F. A.: Kinetics of Diffusional Motion of Pores in Solids. J. Nucl. Mat., vol. 30, no. 1/2, Apr. 1969, pp. 143-165.
3. Carroll, R. M.; and Sisman, O.: Evaluating Fuel Behavior During Irradiation by Fission-Gas Release. Rep. ORNL-4601, Oak Ridge National Lab., Sept. 1970.
4. Kirchgessner, Thomas A.; Weinstein, Michael B.; and Tambling, Thomas N.: A Sweep Gas Facility for Fission Gas Release Studies at the NASA Plum Brook Reactor. NASA TM X-2267, 1971.
5. Weinstein, Michael B.; Kirchgessner, Thomas A.; and Tambling, Thomas N.: Fission-Gas Release From Uranium Nitride at High Fission-Rate Density. NASA TN D-7171, 1973.
6. Carroll, R. M.: Fission-Gas Effects in Reactor Fuels - Part II. Engineering Applications. Nucl. Safety, vol. 12, no. 6, Nov.-Dec. 1971, pp. 562-568.
7. Duncombe, E.; Freidrich, C. M.; and Guilinger, W. H.: An Analytic Model for the Prediction of In-Pile Behavior of Oxide Fuel Rods. Nucl. Tech., vol. 12, no. 2, Oct. 1971, pp. 194-208.
8. Ainscough, J. B.: Some Limiting Aspects of UO_2 Performance. TRG Rep. 1937(s), United Kingdom Atomic Energy Authority, Sept. 29, 1969.
9. Evans, Robley D.: The Atomic Nucleus. McGraw-Hill Book Co., Inc., 1955.
10. Lietzke, Armin F.: Simplified Analysis of Nuclear Fuel Pin Swelling. NASA TN D-5609, 1970.
11. Scarborough, James B.: Numerical Mathematical Analysis. Second ed., Johns Hopkins Press, 1950.
12. Rainville, Earl D.: Elementary Differential Equations. Second ed., Macmillan Co., 1958.
13. Mendelson, Alexander: Plasticity: Theory and Application. Macmillan Co., 1968.
14. Faupel, Joseph H.: Engineering Design. John Wiley & Sons, Inc., 1964.
15. Anon.: Advanced Materials Program for March and April, 1964. Rep. PWAC-1014, Pratt & Whitney Aircraft, June 15, 1964.
16. Anon.: Advanced Materials Program for November and December, 1964. Rep. PWAC-1018. Pratt & Whitney Aircraft, Jan. 27, 1965.

17. Weaver, S. C.; Scott, J. L.; Senn, R. L.; and Montgomery, B. H.: Effects of Irradiation on Uranium Nitride Under Space-Reactor Conditions. Rep. ORNL-4461, Oak Ridge National Lab., Oct. 1969.

18. Patriarca, P.; and Rucker, D. J.: Fuels and Materials Development Program Quarterly Progress Report for Period ending June 30, 1969. Rep. ORNL-4440, Oak Ridge National Lab., Oct. 1969.

19. Patriarca, P.; and Rucker, D. J.: Fuels and Materials Development Program Quarterly Progress Report for Period Ending September 30, 1969. Rep. ORNL-4480, Oak Ridge National Lab., Feb. 1970.

20. Padel, A.; and De Novion, CH.: Constantes Elastiques des Carbures, Nitrures et Oxydes d'Uranium et de Plutonium. J. Nucl. Mat., vol. 33, no. 1, Oct. 1969, pp. 40-51.

21. Hall, A. R.: Elastic Moduli and Internal Friction of Some Uranium Ceramics. J. Nucl. Mat., vol. 37, no. 3, Dec. 1970, pp. 314-323.

22. Anon.: Aerospace Structural Metals Handbook. Vol. IIA: Non-ferrous Alloys. Belfour Stulen, Inc., (AFML-TR-68-115).

23. Moorhead, Paul E.; and Stone, Phillip L.: Survey of Properties of T-111 (Tantalum-8 Tungsten-2 Hafnium). NASA TN D-5873, 1970.

24. Fassler, M. H.; Huegel, F. J.; and DeCrescente, M. A.: Compressive Creep of UC and UN. Rep. PWAC-482, Pt. 1, Pratt & Whitney Aircraft, Oct. 1965.

25. Maag, William L.; and Mattson, William F.: Statistical Analysis of High-Temperature Creep-Rate Data for Alloys of Tantalum, Molybdenum, and Columbium. NASA TN D-5424, 1969.

NATIONAL AERONAUTICS AND SPACE ADMINISTRATION
WASHINGTON, D.C. 20546

OFFICIAL BUSINESS
PENALTY FOR PRIVATE USE $300

SPECIAL FOURTH-CLASS RATE
BOOK

POSTAGE AND FEES PAID
NATIONAL AERONAUTICS AND
SPACE ADMINISTRATION
451

U.S.MAIL

POSTMASTER : If Undeliverable (Section 158 Postal Manual) Do Not Return

"The aeronautical and space activities of the United States shall be conducted so as to contribute . . . to the expansion of human knowledge of phenomena in the atmosphere and space. The Administration shall provide for the widest practicable and appropriate dissemination of information concerning its activities and the results thereof."

—NATIONAL AERONAUTICS AND SPACE ACT OF 1958

NASA SCIENTIFIC AND TECHNICAL PUBLICATIONS

TECHNICAL REPORTS: Scientific and technical information considered important, complete, and a lasting contribution to existing knowledge.

TECHNICAL NOTES: Information less broad in scope but nevertheless of importance as a contribution to existing knowledge.

TECHNICAL MEMORANDUMS: Information receiving limited distribution because of preliminary data, security classification, or other reasons. Also includes conference proceedings with either limited or unlimited distribution.

CONTRACTOR REPORTS: Scientific and technical information generated under a NASA contract or grant and considered an important contribution to existing knowledge.

TECHNICAL TRANSLATIONS: Information published in a foreign language considered to merit NASA distribution in English.

SPECIAL PUBLICATIONS: Information derived from or of value to NASA activities. Publications include final reports of major projects, monographs, data compilations, handbooks, sourcebooks, and special bibliographies.

TECHNOLOGY UTILIZATION PUBLICATIONS: Information on technology used by NASA that may be of particular interest in commercial and other non-aerospace applications. Publications include Tech Briefs, Technology Utilization Reports and Technology Surveys.

Details on the availability of these publications may be obtained from:

SCIENTIFIC AND TECHNICAL INFORMATION OFFICE

NATIONAL AERONAUTICS AND SPACE ADMINISTRATION

Washington, D.C. 20546